NAVAL POSTGRADUATE SCHOOL
Monterey, California

THESIS

THE CONTRIBUTION OF SYMMETRIZATION TO THE INTENSIFICATION OF TROPICAL CYCLONES

by

Henry A. Miller

December 2001

Thesis Advisor: Roger T. Williams
Second Reader: Chih-Pei Chang

Approved for public release; distribution is unlimited.

Report Documentation Page

Report Date	Report Type	Dates Covered (from... to)
19 Dec 2001	N/A	-

Title and Subtitle	Contract Number
The Contribution of Symmetrization to the Intensification of Tropical Cyclones	Grant Number
	Program Element Number

Author(s)	Project Number
Miller, Henry	Task Number
	Work Unit Number

Performing Organization Name(s) and Address(es)	Performing Organization Report Number
Naval Postgraduate School Monterey, California	

Sponsoring/Monitoring Agency Name(s) and Address(es)	Sponsor/Monitor's Acronym(s)
	Sponsor/Monitor's Report Number(s)

Distribution/Availability Statement
Approved for public release, distribution unlimited

Supplementary Notes
The original document contains color images.

Abstract

Subject Terms

Report Classification	Classification of this page
unclassified	unclassified

Classification of Abstract	Limitation of Abstract
unclassified	UU

Number of Pages
69

THIS PAGE INTENTIONALLY LEFT BLANK

REPORT DOCUMENTATION PAGE		*Form Approved OMB No. 0704-0188*
Public reporting burden for this collection of information is estimated to average 1 hour per response, including the time for reviewing instruction, searching existing data sources, gathering and maintaining the data needed, and completing and reviewing the collection of information. Send comments regarding this burden estimate or any other aspect of this collection of information, including suggestions for reducing this burden, to Washington headquarters Services, Directorate for Information Operations and Reports, 1215 Jefferson Davis Highway, Suite 1204, Arlington, VA 22202-4302, and to the Office of Management and Budget, Paperwork Reduction Project (0704-0188) Washington DC 20503.		
1. AGENCY USE ONLY *(Leave blank)*	**2. REPORT DATE** December 2001	**3. REPORT TYPE AND DATES COVERED** Master's Thesis
4. TITLE AND SUBTITLE: The Contribution of Symmetrization to the Intensification of Tropical Cyclones		**5. FUNDING NUMBERS**
6. AUTHOR(S) Miller, Henry A.		
7. PERFORMING ORGANIZATION NAME(S) AND ADDRESS(ES) Naval Postgraduate School Monterey, CA 93943-5000		**8. PERFORMING ORGANIZATION REPORT NUMBER**
9. SPONSORING /MONITORING AGENCY NAME(S) AND ADDRESS(ES) N/A		**10. SPONSORING/MONITORING AGENCY REPORT NUMBER**
11. SUPPLEMENTARY NOTES The views expressed in this thesis are those of the author and do not reflect the official policy or position of the Department of Defense or the U.S. Government.		
12a. DISTRIBUTION / AVAILABILITY STATEMENT Approved for public release; distribution is unlimited.		**12b. DISTRIBUTION CODE**

13. ABSTRACT *(maximum 200 words)*

Operational ability to forecast tropical cyclone motion is much better than the ability to forecast intensity change. Several recent works have studied the mechanisms that bring about the symmetrization of various types of asymmetries in tropical cyclones. This study was conducted to add to that knowledge by examining the transfers of kinetic energy between scales and how those energy transfers alter the wind structure of the cyclone. Adding to the understanding of how this process can alter winds is a step toward increasing ability to forecast these changes.

A non-divergent barotropic spectral model was used to integrate annular bands of enhanced potential vorticity, simulating hurricane eyes, with varying degrees of offset from the center of the vortex. Offset monopoles of vorticity, simulating asymmetric convection in tropical storms, were also integrated. As discovered by previous researchers, these unstable eyes broke down into a series of mesovortices, which merged and eventually relaxed to monopolar or tripolar final states. The offset monopoles formed spiral bands and became symmetric as well. Kinetic energy was transferred from the mean flow to the asymmetries as mesovortices formed and then transferred back to the mean flow as symmetrization occurred. These energy transfers occurred very quickly. As energy was transferred from asymmetry to mean flow, the azimuthally averaged wind increased in a band of about 70 km from the center of the vortex, even though the maximum wind decreased. Azimuthally averaged wind in the monopole cases also increased, but the change was confined to a smaller radial band near the radius of maximum wind.

14. SUBJECT TERMS Tropical Cyclone Intensity, Asymmetric Convection, Mesovortices, Kinetic Energy Transfers in Tropical Cyclones			**15. NUMBER OF PAGES** 69
			16. PRICE CODE
17. SECURITY CLASSIFICATION OF REPORT Unclassified	**18. SECURITY CLASSIFICATION OF THIS PAGE** Unclassified	**19. SECURITY CLASSIFICATION OF ABSTRACT** Unclassified	**20. LIMITATION OF ABSTRACT** UL

NSN 7540-01-280-5500

Standard Form 298 (Rev. 2-89)
Prescribed by ANSI Std. 239-18

i

THIS PAGE INTENTIONALLY LEFT BLANK

THE CONTRIBUTION OF SYMMETRIZATION TO THE INTENSIFICATION OF TROPICAL CYCLONES

Henry A. Miller
Lieutenant Commander, United States Navy
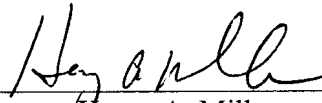B.S., United States Naval Academy, 1990

Submitted in partial fulfillment of the
requirements for the degree of

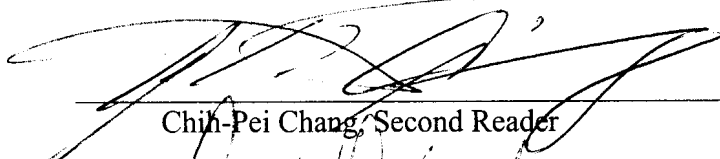## MASTER OF SCIENCE METEOROLOGY AND PHYSICAL OCEANOGRAPHY

from the

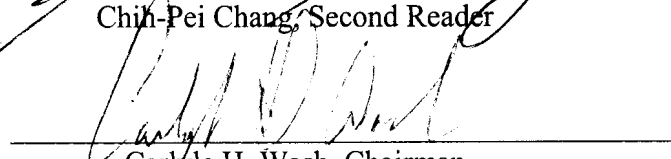## NAVAL POSTGRADUATE SCHOOL
December 2001

Author: _____
Henry A. Miller

Approved by: _____
Roger T. Williams, Thesis Advisor

_____
Chih-Pei Chang, Second Reader

_____
Carlyle H. Wash, Chairman
Department of Meteorology

THIS PAGE INTENTIONALLY LEFT BLANK

ABSTRACT

Operational ability to forecast tropical cyclone motion is much better than the ability to forecast intensity change. Several recent works have studied the mechanisms that bring about the symmetrization of various types of asymmetries in tropical cyclones. This study was conducted to add to that knowledge by examining the transfers of kinetic energy between scales and how those energy transfers alter the wind structure of the cyclone. Adding to the understanding of how this process can alter winds is a step toward increasing ability to forecast these changes.

A non-divergent barotropic spectral model was used to integrate annular bands of enhanced potential vorticity, simulating hurricane eyes, with varying degrees of offset from the center of the vortex. Offset monopoles of vorticity, simulating asymmetric convection in tropical storms, were also integrated. As discovered by previous researchers, these unstable eyes broke down into a series of mesovortices, which merged and eventually relaxed to monopolar or tripolar final states. The offset monopoles formed spiral bands and became symmetric as well. Kinetic energy was transferred from the mean flow to the asymmetries as mesovortices formed and then transferred back to the mean flow as symmetrization occurred. These energy transfers occurred very quickly. As energy was transferred from asymmetry to mean flow, the azimuthally averaged wind increased in a band of about 70 km from the center of the vortex, even though the maximum wind decreased. Azimuthally averaged wind in the monopole cases also increased, but the change was confined to a smaller radial band near the radius of maximum wind.

THIS PAGE INTENTIONALLY LEFT BLANK

TABLE OF CONTENTS

THIS PAGE INTENTIONALLY LEFT BLANK

LIST OF FIGURES

LIST OF TABLES

THIS PAGE INTENTIONALLY LEFT BLANK

ACKNOWLEDGMENTS

I would like to thank my thesis advisor, Dr. R. T. Williams, for his guidance through this project. Dr. Hung-Chi Kuo was also invaluable in helping design the experiments, providing the model used in the study, and in interpreting results. Bob Creasey was a lifesaver at resolving my many computer problems and provided much needed disk space. Arlene Guest and Mike Cook answered at least a million FORTRAN and MATLAB questions. I appreciate my classmates Marc Eckardt and Cathy McDougall for always being around so we could confer on the little questions and provide each other encouragement. Finally, I thank my wife, Deena, for her support through this thesis and the entire master's degree program.

THIS PAGE INTENTIONALLY LEFT BLANK

I.   INTRODUCTION

Tropical cyclones are typically quite symmetric vortices in their mature state. However, asymmetries such as offset areas of intense convection and off-center eyes do frequently occur. An example of asymmetric convection is Hurricane Georges, shown in Figure 1. In Hurricane Bonnie, a typical example of an off-center eye case, the eye is quite far off-center at 2345UTC 15AUG98 in Figure 2a, yet it has become completely symmetrical three days later, shown in Figure 2b. These types of asymmetric patterns can become quite symmetric in a short period of time (Prieto, et. al., 2001). Numerous recent studies have sought to explain the formation processes, behavior, and axisymmetrization mechanisms of various asymmetries in tropical cyclones including asymmetric convection, offset eyes, polygonal eyewall features, and spiral bands.
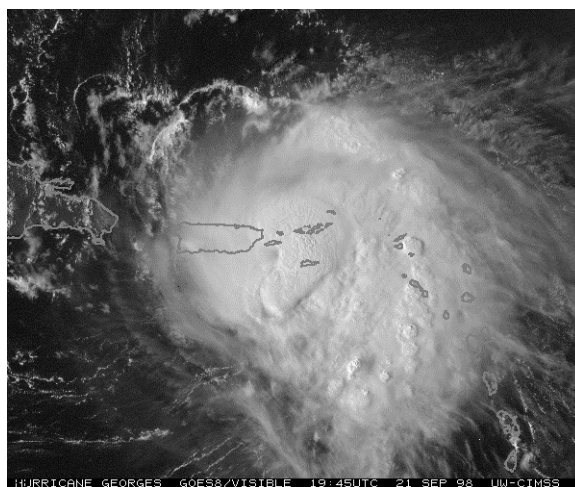
Figure 1. GOES 8 visible imagery of Hurricane Georges 1945UTC 21SEP98 from UW-CIMSS web site http://cimss.ssec.wisc.edu/tropic/archive/1998/storms/georges/ .

Kossin and Schubert (2001) studied the mechanisms of formation of mesovortices and polygonal features. An eyewall was simulated using an annular ring of enhanced vorticity in a barotropic pseudospectral model. This unstable eyewall broke down into a series of mesovortices, which subsequently merged. Depending upon the initial conditions used, the series of mesovortices relaxed to either a monopole or a rotating asymmetric quasi-steady state.

1
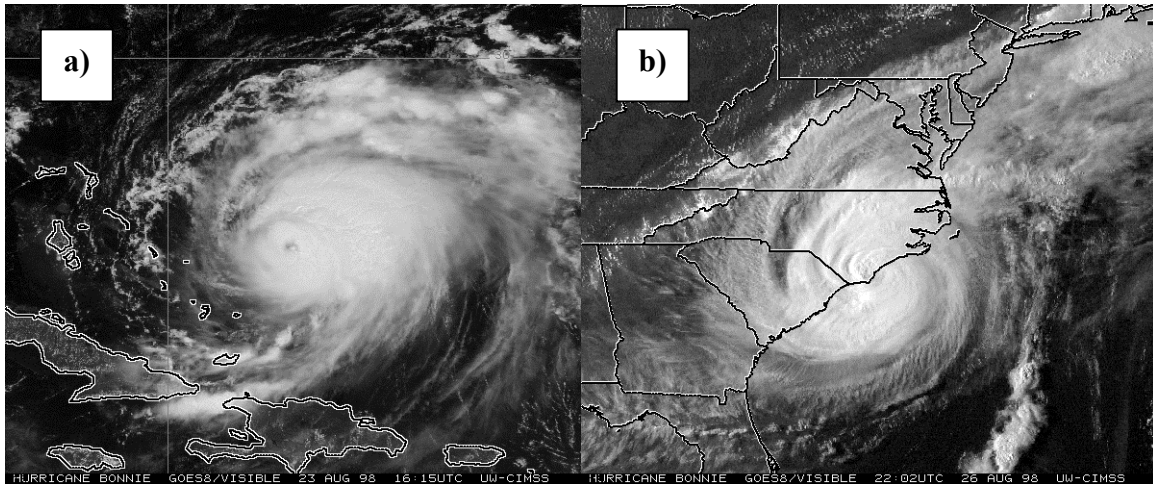
Figure 2. GOES 8 visible imagery of Hurricane Bonnie from UW-CIMSS web site
http://cimss.ssec.wisc.edu/tropic/archive/1998/storms/bonnie/. a) 1615UTC 23AUG98 showing a
very off-center eye. b) Three days later at 2201UTC 26AUG98 with a highly symmetric
form.

Kuo, et. al. (1999) explored elliptical and polygonal eyewalls based on observations of a rotating elliptical eyewall in Typhoon Herb. Previous work, including that of Lewis and Hawkins (1982), Kurihara (1976) and Willoughby (1978), has sought to explain the mechanics of this type of feature. The Kuo study used both linear and non-linear theory, along with numerical computations, to demonstrate the processes of neutral vorticity wave interactions, vorticity redistribution, wave breaking, and vortex merging in supporting the rotation of the asymmetric eye.

The formation and maintenance of asymmetric spiral bands were studied by Chen and Yau (2001). This study used the PSU-NCAR nonhydrostatic mesoscale model (MM5) to integrate an initially axisymmetric vortex forward in time and explore the formation of asymmetric bands. The researchers found that, in addition to the continuous generation of potential vorticity by latent heat release, the inward transport of potential vorticity by vortex Rossby waves and non-linear mixing tend to increase the vorticity in the inner core region and intensify the hurricane. At the same time, frictional processes and linear potential vorticity mixing tend to weaken the hurricane.

Schubert, et. al. (1999) presented a study of the formation and axisymmetrization mechanics of mesovortices and polygonal eyewall features. These researchers reviewed

linear theory and then performed simulations using a barotropic pseudospectral numerical model. They found that due to barotropic instability, eyewalls may break down into mesovortices. Vorticity then pools into discrete regions around the inner core of the vortex causing a polygonal eyewall. Eventually, vorticity stabilized into a symmetric monopole structure.

Prieto, et. al. (2001, hereafter PKS) used a nondivergent barotropic model to study the axisymmetrization processes of offset monopoles of vorticity and off-center eyes. Several experiments were conducted using varying degrees of offset of the monopoles and eyes. They showed that due to barotropic instability, unstable hurricane eyewalls can break down into mesovortices. Vortex Rossby waves, wave dynamics, and production and subsequent break up of spiral bands and filaments contribute to the redistribution of vorticity and produce an end-state of a tripolar structure or a symmetric monopole.

Each of these previous studies explored some aspect of the formation, maintenance, or axisymmetrization of the asymmetric features of tropical cyclones. The objective of this study is to build upon the knowledge provided by these and other works by considering transfer of kinetic energy between the asymmetric features and the symmetric mean flow of the tropical cyclone. According to Bosart, et. al. (2000), all processes that affect intensification of tropical cyclones fall into three broad categories: 1) large-scale environmental influences, 2) storm-scale internal dynamics, and 3) ocean-atmosphere interactions. The transfer of kinetic between the symmetric mean flow and perturbations represents a storm-scale internal dynamic process. A more thorough understanding of this transfer of energy can provide insights into how the development and subsequent axisymmetrization of asymmetric features affects the intensification process.

In a paper that has become a classic, Lorenz (1960) postulated that any atmospheric system of any scale possesses a given amount of kinetic energy. In order for the system to develop, potential or internal energy must be converted to kinetic energy within the system or kinetic energy must be transferred to the system from some other system. The study is conducted using a non-divergent barotropic model. Since the model cannot represent potential and internal energy, the study considers only the

transfer of kinetic energy from one system to another, or in this case, from the smaller scale asymmetries to the larger scale mean circulation of the tropical cyclone.

As stated by Kossin and Schubert (2001), the non-conservative boundary layer and moist processes play a significant role in the evolution of a tropical cyclone. However, it is still very useful to study cyclone development using a simplified model, which cannot simulate these processes. Using the non-divergent, barotropic model allows the effects of conservative processes to be isolated from the effects of the more complex physics. Since the simplified model does not represent the non-conservative processes, it is much easier to determine the mechanism causing evolution of the features being studied.

II.   MODEL DESCRIPTION

As the initial conditions used in these experiments contain very sharp gradients in vorticity, the highest possible degree of computational accuracy is desired.   Finite difference discretizations yield algebraic convergence with an error of $O(N^P)$ where N is the degrees of freedom and P is the integer order of the method, typically two or four. Spectral methods, on the other hand, yield exponential convergence with an error of $O(e^{-\alpha N})$ where α is come positive number.   Therefore, the spectral methods provide a much more accurate solution than finite difference methods when using the same number of grid points (Fulton and Schubert, 1987).

The model used in this study is a non-divergent, barotropic spectral model developed by Hung-Chi Kuo (Kuo and Schubert, 1988). It is a channel model with walls in the north and south and uses periodic east and west boundaries such that:

$$\zeta(-1) = \zeta(N-1) \ \text{ and } \ \zeta(0) = \zeta(N)$$

where N is the number of collocation points in the east-west direction.   The spatial discretization is based on Chebyshev polynomial expansion (Orszag, 1971a, b; Orszag and Israeli, 1974) in latitude and Fourier in longitude. This method leads to collocation points that are equally spaced in longitude, but are more closely spaced near the boundaries than in the middle of the grid in latitude. The time discretization is fourth-order Runge-Kutta method, which was found by Fulton and Schubert (1987) to be most efficient when using the Chebyshev methods.

Most of the experiments were conducted using the *f*-plane with the barotropic vorticity equation as the prognostic equation in the model:

$$\frac{D\zeta}{Dt} = \upsilon \nabla^2 \zeta \tag{1}$$

or with the material derivative expanded:

$$\frac{\partial \zeta}{\partial t} + u\frac{\partial \zeta}{\partial x} + v\frac{\partial \zeta}{\partial y} = \upsilon \nabla^2 \zeta \tag{2}$$

A streamfunction ψ is defined such that

$$\zeta = \nabla^2\psi, \qquad u = -\frac{\partial\psi}{\partial y}, \text{ and} \qquad v = \frac{\partial\psi}{\partial x} \qquad \text{(3),(4),(5)}$$

Substituting in the streamfunction definitions and using the Jacobian operator, the barotropic vorticity equation becomes:

$$\frac{\partial\zeta}{\partial t} + J(\psi,\zeta) = \upsilon\nabla^2\zeta \qquad \text{(6)}$$

Several runs were made using the β plane model for comparison against the f-plane cases. In the β plane model, the barotropic vorticity equation becomes:

$$\frac{\partial\zeta}{\partial t} + J(\psi,\zeta) + \beta\frac{\partial\psi}{\partial x} = \upsilon\nabla^2\zeta \qquad \text{(7)}$$

The value of $\beta = 2.205\times10^{-11}m^{-1}s^{-1}$ was chosen by fixing 15° as the center latitude of the vortex and using the equation:

$$\beta = \frac{2\omega\cos\phi}{a} \qquad \text{(8)}$$

where ω is the angular rate of rotation of earth, ϕ is latitude, and a is the radius of earth. A viscosity of $\upsilon = 6.5m^2s^{-1}$ was used for all runs, both f-plane and β plane.

One of the early principles of numerical weather prediction is that total energy should be conserved for reversible adiabatic processes (Lorenz, 1960). In the barotropic model, there is no representation of internal or potential energy, so kinetic energy should conserved as nearly as possible. Kinetic energy is calculated by

$$KE = \iint \tfrac{1}{2}(u^2 + v^2)dxdy \qquad \text{(9)}$$

Figure 3 shows the kinetic energy decay for Experiment D. In this case, which was the initially symmetric monopole control run, kinetic energy decay of 2.4% over 50 hours was the greatest of all experiments conducted. To determine how much of the decay was due to the viscosity used in the model, this experiment was repeated with $\upsilon = 0$. Kinetic energy decreased only 0.012%, as shown in Figure 4, effectively demonstrating that all

6

energy loss in these experiments is due to the viscosity term.   It should be noted that even though kinetic energy is not completely conserved when viscosity is used, the
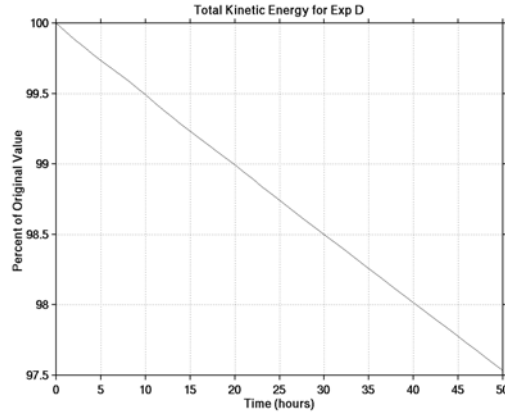
Figure 3. Decay of total kinetic energy over the domain for Experiment D with viscosity included in the model.
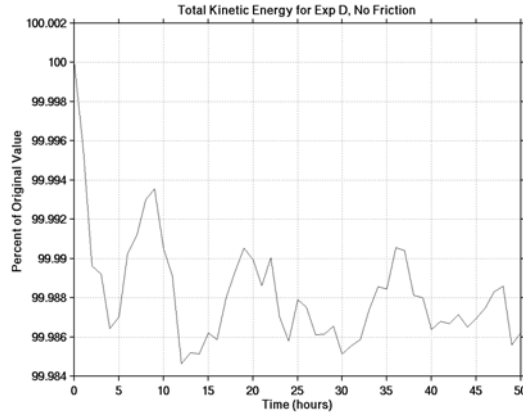
Figure 4. Decay of total kinetic energy over the domain for Experiment D with no viscosity included in the model.

viscosity is necessary in order to reach a steady-state condition. Without viscosity, the pattern never becomes completely smooth. This effect is discussed more fully in Section III.C.4.

Enstrophy

$$Z = \iint \tfrac{1}{2} \zeta^2 \, dx \, dy \qquad (10)$$

7

is also calculated for each output time for all experiments. Enstrophy is plotted as a function of time to show the cascade of vorticity to smaller scales.

Unless otherwise noted, the model was run with a physical domain of 216×216 km. The vorticity monopole experiments used 216×216 collocation points with 144×144 Fourier modes resulting in an effective dealiased resolution of 1.5 km. These experiments were run with a 30 second time step. The eye experiments used 432×432 collocation points and 288×288 Fourier modes for a 0.75 km resolution. The time step for these experiments was 10 seconds.

III.   NUMERICAL RESULTS

A.   OFFSET EYE EXPERIMENTS

1.   Initial Conditions

The initial conditions for the offset eye experiments are the same as those used by PKS, though not all variations explored in that research are presented in this paper. In each of these experiments, the eye is represented as a circular region of lower, constant vorticity surrounded by an annular ring of elevated vorticity that decreases with distance from the eye.

The initial vorticity field for this set of experiments is given by

$$\zeta(x,y,0) = \zeta_e + \begin{cases} \zeta_1, & 0 \le \hat{r} \le r_1 \\ \zeta_1 S\left(\dfrac{\hat{r}-r_1}{d_1}\right) + \zeta_2 S\left(\dfrac{r_1-\hat{r}}{d_1}\right), & r_1 \le \hat{r} \le (r_1+d_1) \\ \zeta_2, & (r_1+d_1) \le \hat{r} \ and \ r \le r_2 \\ \zeta_2 S\left(\dfrac{r-r_2}{d_2}\right), & r_2 \le r \le (r_2+d_2) \\ 0, & otherwise \end{cases}$$

where

$$\hat{r} = \sqrt{(x-x_0)^2 + y^2} \qquad \text{and} \qquad r = \sqrt{x^2 + y^2}$$

The values for r_1, r_2, x_0, d_1, d_2, ζ_1, and ζ_2 are all independently specified. The value of ζ_e is chosen such that the average vorticity over the domain is zero, resulting in a small negative vorticity outside the vortex. The function *S(s)* is the basic cubic Hermite shape function

$$S(s) = 1 - 3s^2 + 2s^3$$

This procedure with a uniform small negative vorticity ζ_e outside the area of positive vorticity produces nearly irrotational flow in the corners of the domain since streamfunction is the solution to a Poisson equation with small forcing.

9
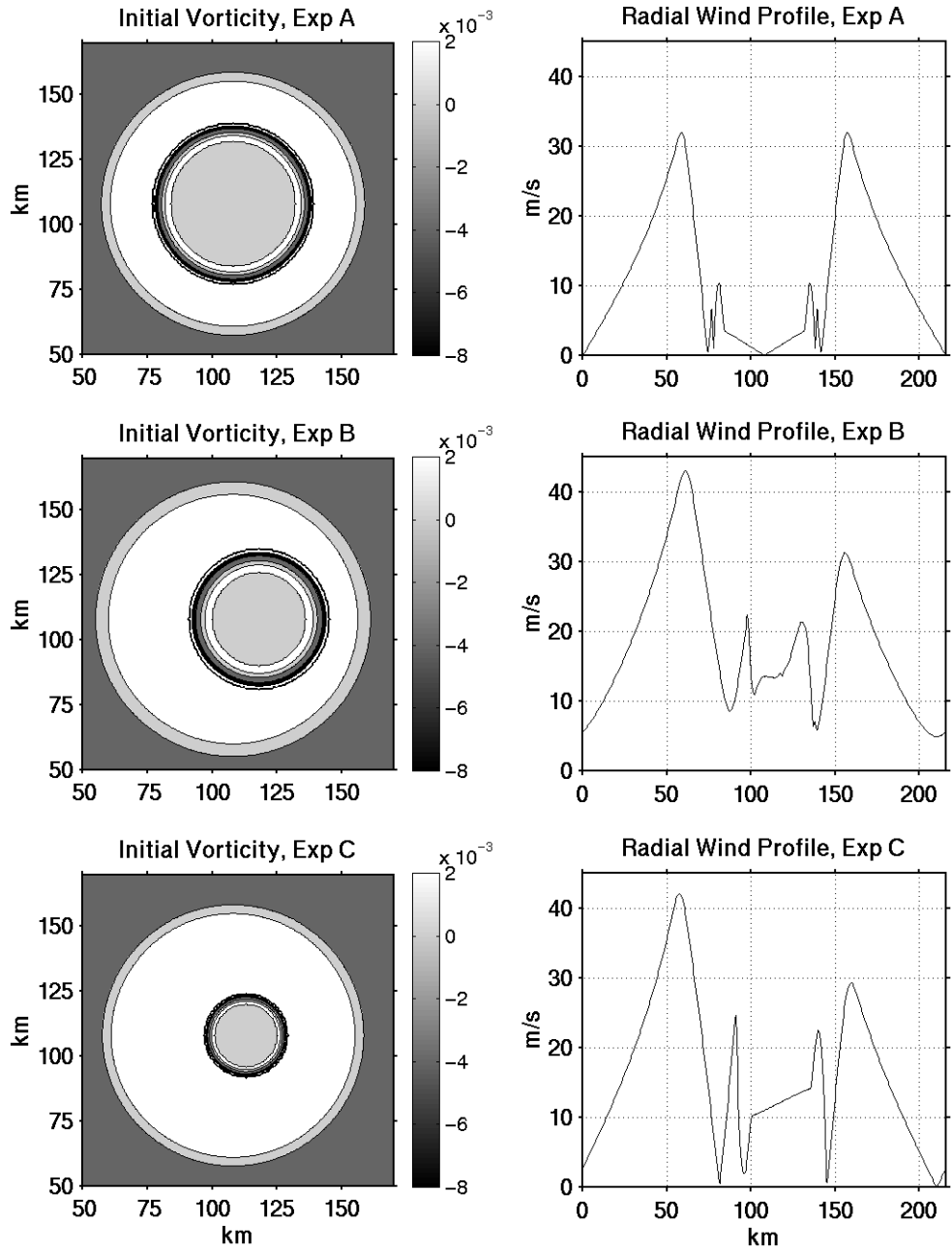
Figure 5. Initial vorticity field and wind profile for all monopole experiments. The wind profile shown is taken east-west across the center of the vortex.

First a control run, Experiment A, was conducted using a large symmetric eye. Experiment B was a medium offset eye and Experiment C was a small offset eye. The values used for each of these parameters for each of the eye experiments are given in Table 1 below. The initial vorticity field and a corresponding profile of winds across the vortex is shown for each of these experiments in Figure 5.

Exp.	r_1	r_2	x_0	d_1	d_2	ζ_e	ζ_1	ζ_2	PKS Exp.
	(km)	(km)	(km)	(km)	(km)	$(x10^{-5}s^{-1})$	$(x10^{-5}s^{-1})$	$(x10^{-5}s^{-1})$	
A	24	45	0	7	7	-26.7	60	300	D2
B	18	45	10	9	10	-32.7	60	300	E
C	12	45	5	4	7	-41.9	60	300	F

Table 1.   Initial condition parameters for offset eye experiments.

2.   Vorticity Structure Evolution

The vorticity evolution was qualitatively similar to that of PKS in each experiment where identical initial conditions were used. Though there were some differences in the structures that evolved, the most significant difference was that development occurred faster. The models used in their study and this one were both non-divergent, barotropic spectral models, but there were two key differences which probably led to the differences in development. The model used by PKS was a doubly periodic Fourier model, while the one used in this study used the Fourier-Chebyshev method. The domain used in the previous study was 200x200 km while this one was 216x216 km. Since the formulation of the initial conditions sets the background vorticity such that average vorticity over the domain is zero, the background vorticity in these experiments was a larger negative value than that used by PKS.

Figures 6 and 7 show the evolution of the vorticity pattern for Experiment A, which was the large eye that was initially symmetric. Schubert, et. al. (1999) conducted an experiment with similar initial conditions, but with a wider band of elevated vorticity

11

surrounding the eye. PKS actually give little information about their experiment with these initial conditions except that the results were similar to Schubert and that the final
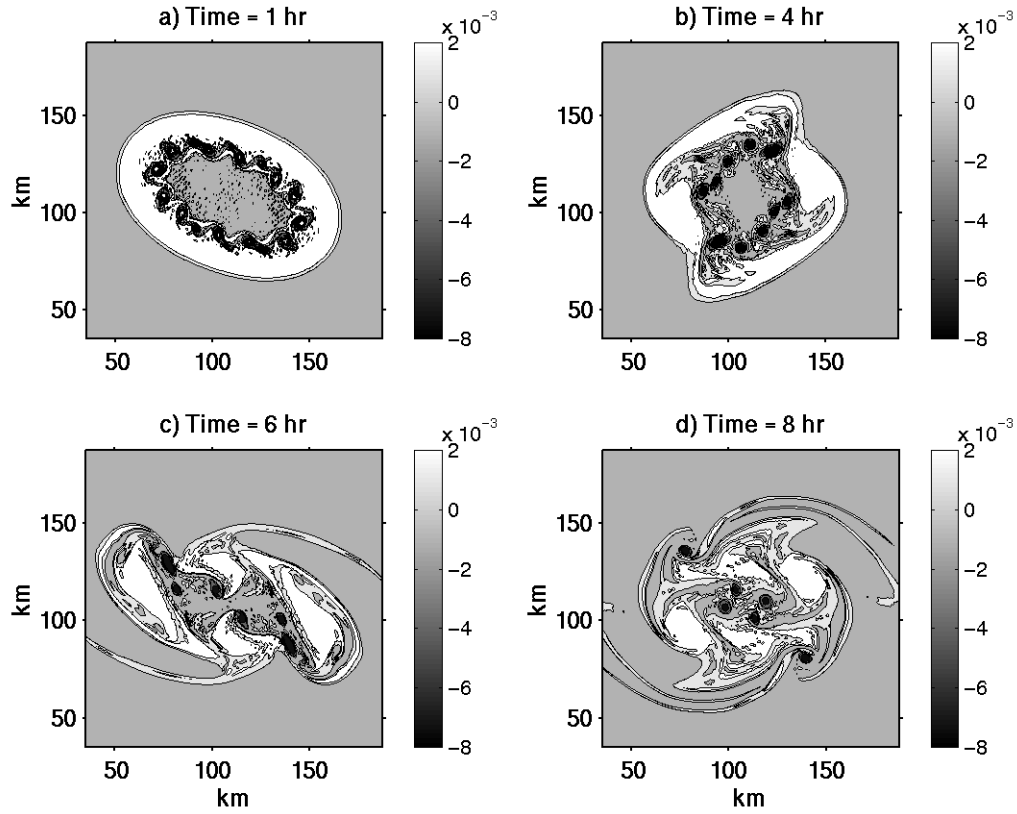
Figure 6. Vorticity fields for Experiment A at a) one hour, b) four hours, c) six hours, and d) eight hours.

equilibrium state was a tripole structure. Though PKS reports results similar to Schubert, et. al., the end state was a tripole, while the Schubert, et. al. end state was monopolar. The results from this experiment were similar to both PKS and Schubert, et. al. as wave breaking occurred early, in fact earlier than in either of the previous studies, and the equilibrium state was a tripole structure.

By one hour, wave breaking occurred along the inner wall of the elevated vorticity ring. This wave breaking did not occur until six hours in the Schubert, et. al. study. Additionally, in that study four breaking waves formed while in the current work twelve waves developed. It should be noted that the Schubert, et. al. study used a grid spacing of four km, while the current work used one km spacing. Wave breaking

occurred along the outer wall of the ring at four hours, while the outer waves broke at eight hours in the previous work. By six hours, four pools of vorticity have
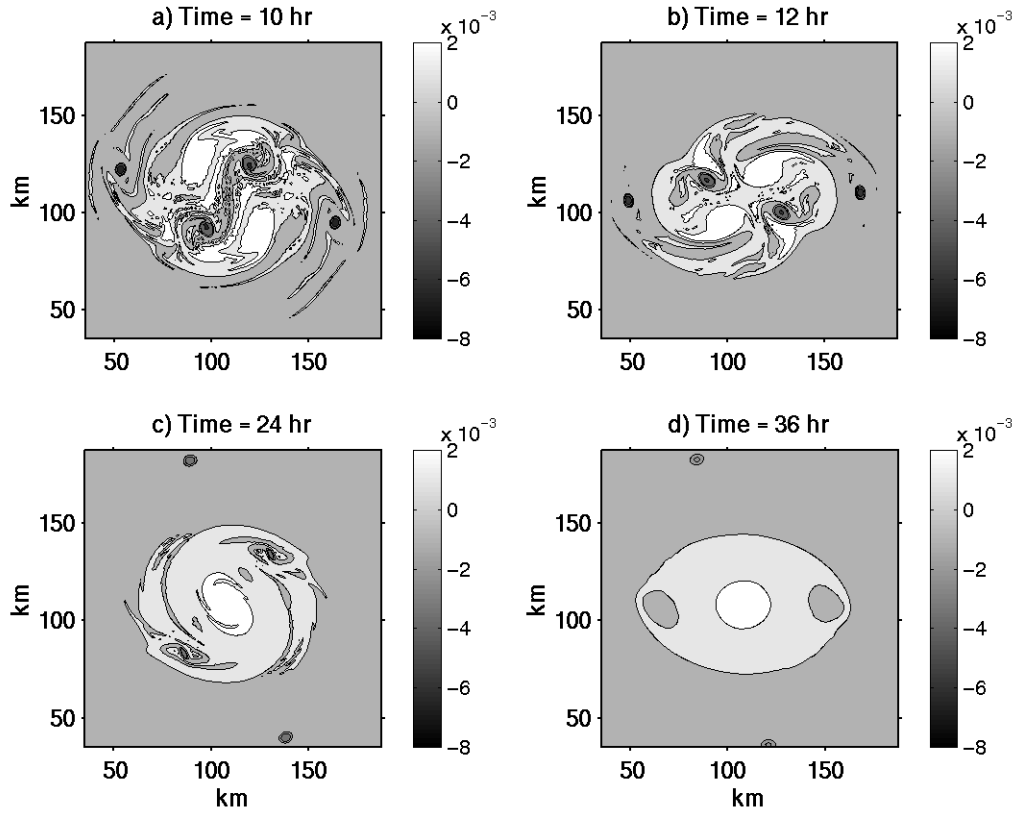
Figure 7. Vorticity fields for Experiment A at a) 10 h, b) 12 h, c) 24 h, and d) 36 h.

formed and at twelve hours, two small pools of negative vorticity form and orbit the vortex for the remainder of the model run. The central tripole formed by 24 h, though its structure became much smoother as time passed. By 36 h, the structure of both the central tripole and the satellites of negative vorticity are very smooth and simply rotate for the rest of the model run. This is the final quasi-steady state.

Schubert, et. al. discussed an enstrophy cascade at eight hours when the violent wave breaking occurred. This experiment also resulted in a significant decay of enstrophy, shown in Figure 8. The enstrophy decay began immediately and continued until about 10 h while the wave breaking and mixing occurred.

Experiment B is the medium-sized offset eye case, which was run with the same initial conditions as the PKS Experiment E. This case evolved similarly to the PKS
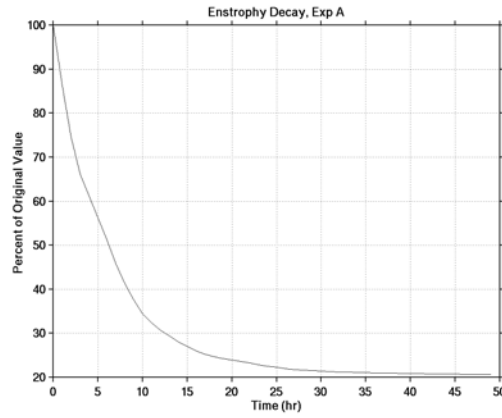
Figure 8. Enstrophy decay for Experiment A.
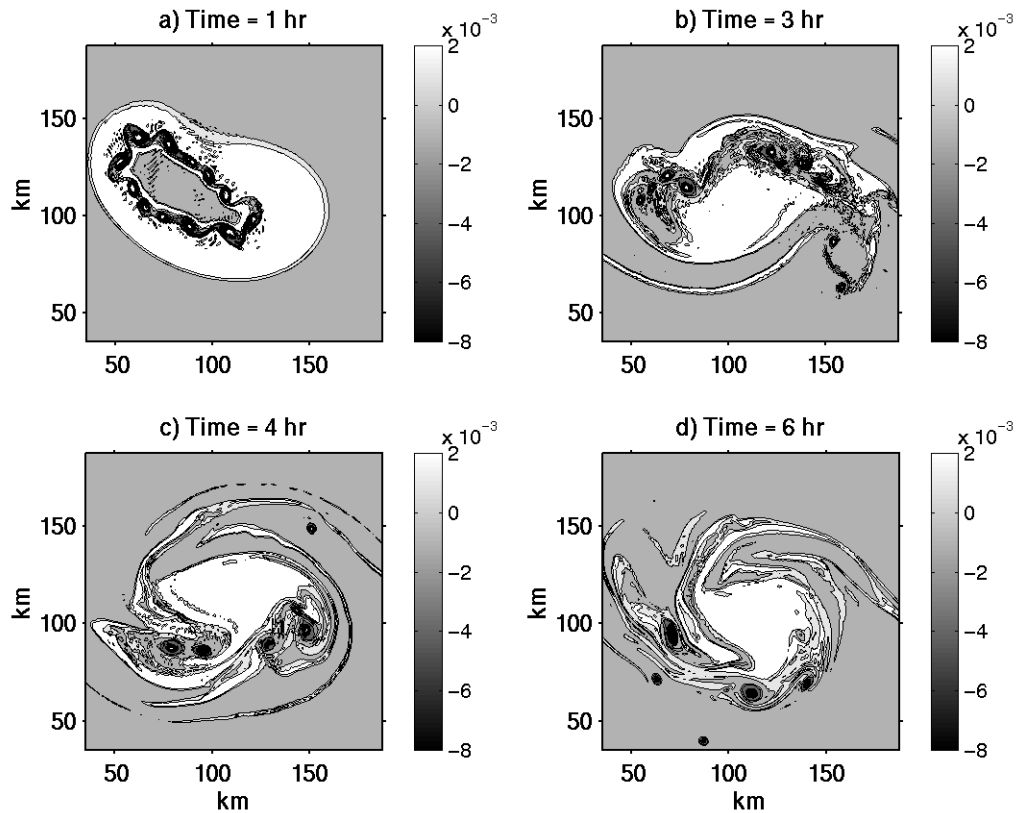
Figure 9. Vorticity fields for Experiment B at a) one hour, b) three hours, c) four hours, and d) six hours.

experiment early in the model run with wave breaking and violent mixing. In the later hours, however, this case evolved into a monopole of positive vorticity with two to four (depending on time) orbiting satellites of negative vorticity, while the PKS experiment developed into a tripolar final state.

The Experiment B vorticity evolution is depicted in Figures 9 and 10. Just as in Experiment A, wave breaking occurred almost immediately and is obvious in Figure 9a at one hour. By three hours, violent mixing has begun and broken apart the outer wall of the elevated vorticity ring. A long thin filament of elevated vorticity fluid formed extending out into the lower vorticity region outside the vortex. Between hours four and seven, strong mixing continued and the central region become very disorganized. Then at hour eight, the central monopole first became organized, though it was quite ragged at this time and gradually became more smooth and circular in the following hours. At twelve hours four small pools of negative formed outside the vortex. These
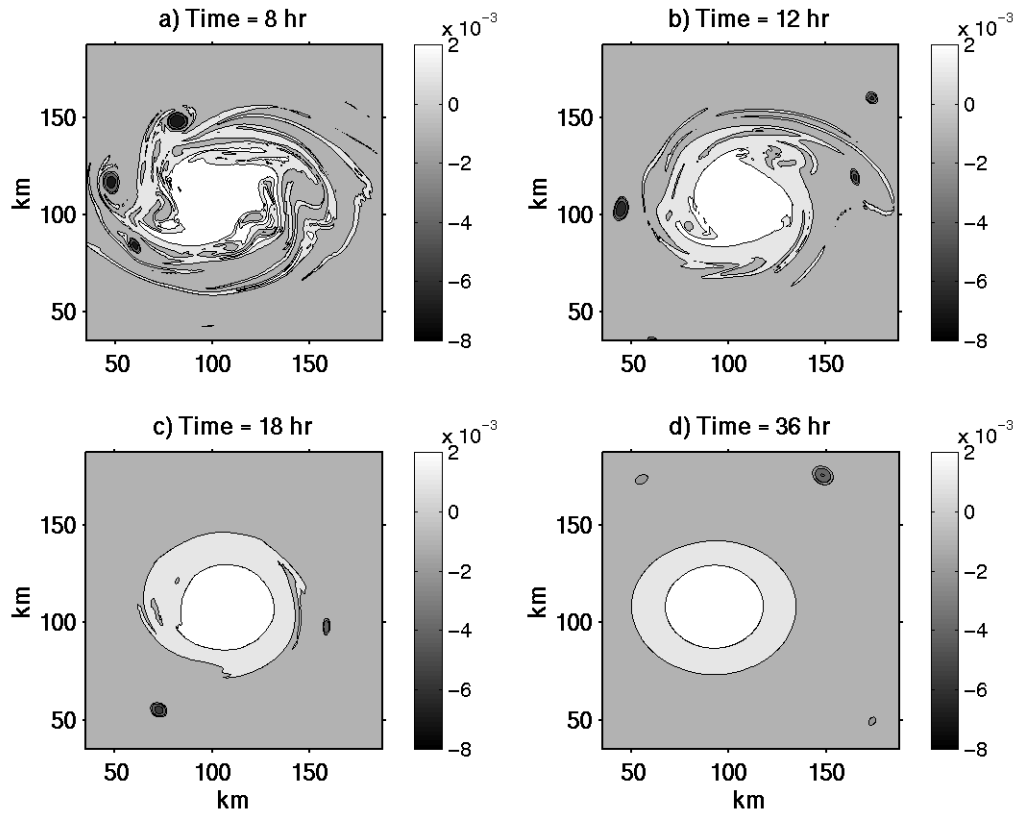
Figure 10. Vorticity fields for Experiment B at a) 8 h, b) 12 h, c) 18 h, and d) 36 h.

15

satellites orbit the vortex and eventually merge into two pools. By 30 h the vortex had become very smooth and slightly elliptical with two satellites of negative vorticity, forming the final quasi-steady state.

Experiment C is the small offset eye using the same initial conditions as PKS's Experiment F. In the PKS experiment, the eye was preserved for the entire model run, though it was farther offset at 72 h than at the beginning. In this experiment, the eye was actually ejected from the vortex at 31 h. The vorticity structure through this experiment is illustrated in Figures 11 and 12.

Just as in the first two experiments, violent mixing through wave breaking along the inner wall occurred during the first hour. At hour four, the outer wall of the ring had distorted toward a triangular shape. Wave breaking began to occur along the outer wall at six hours and a long thin filament developed and extended into the lower vorticity region surrounding the vortex. A second filament formed at hour seven and from hours eight through 24, vorticity was mixed into the outer region as the filaments grew and subsequently broke up in the low vorticity region. A lobe of low vorticity fluid intruded into the vortex at 26 h and by 28 h the eye was pushed to the outer edge of the vortex. The low vorticity fluid which had initially been the eye was squeezed through the outer edge of the vortex and ejected at hours 30 and 31. By hour 42, two smaller poles of positive vorticity formed around the central high vorticity region and persisted for several hours until the structure eventually relaxed to a monopole final state at 68 h.

The enstrophy cascade in the experiment occurred in two stages. First, a sharp decay of enstrophy occurred during the first five hours coincident with the violent mixing around the inner wall of the eye as shown in Figure 13. Afterward the decrease in enstrophy was very gradual until the 25 h point. Between 25 and 32 h a second sharp decrease in enstrophy occurred as low vorticity fluid from the outer region intruded into the vortex and the eye was ejected.

3.   **Wind Profile Evolution and Kinetic Energy Transfers**

As discussed in Section II, the total kinetic energy over the domain is almost conserved, only decaying a small amount due solely to the viscosity used in the model's prognostic equation. In order to analyze the transfer of kinetic energy between the mean

16
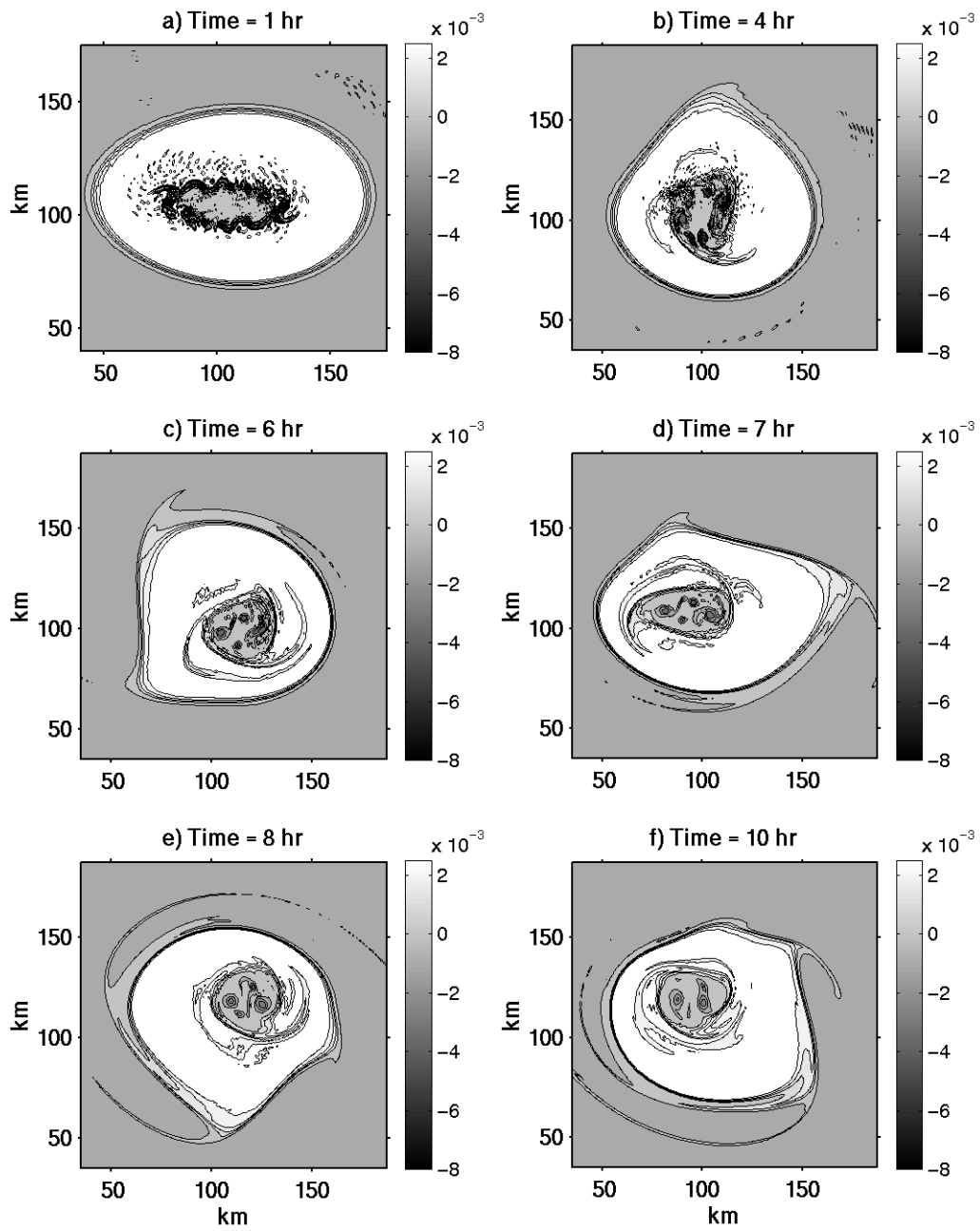
Figure 11. Vorticity fields for Experiment C at a) one hour, b) four hours, c) six hours, d) seven hours, e) eight hours, and f) ten hours.

17
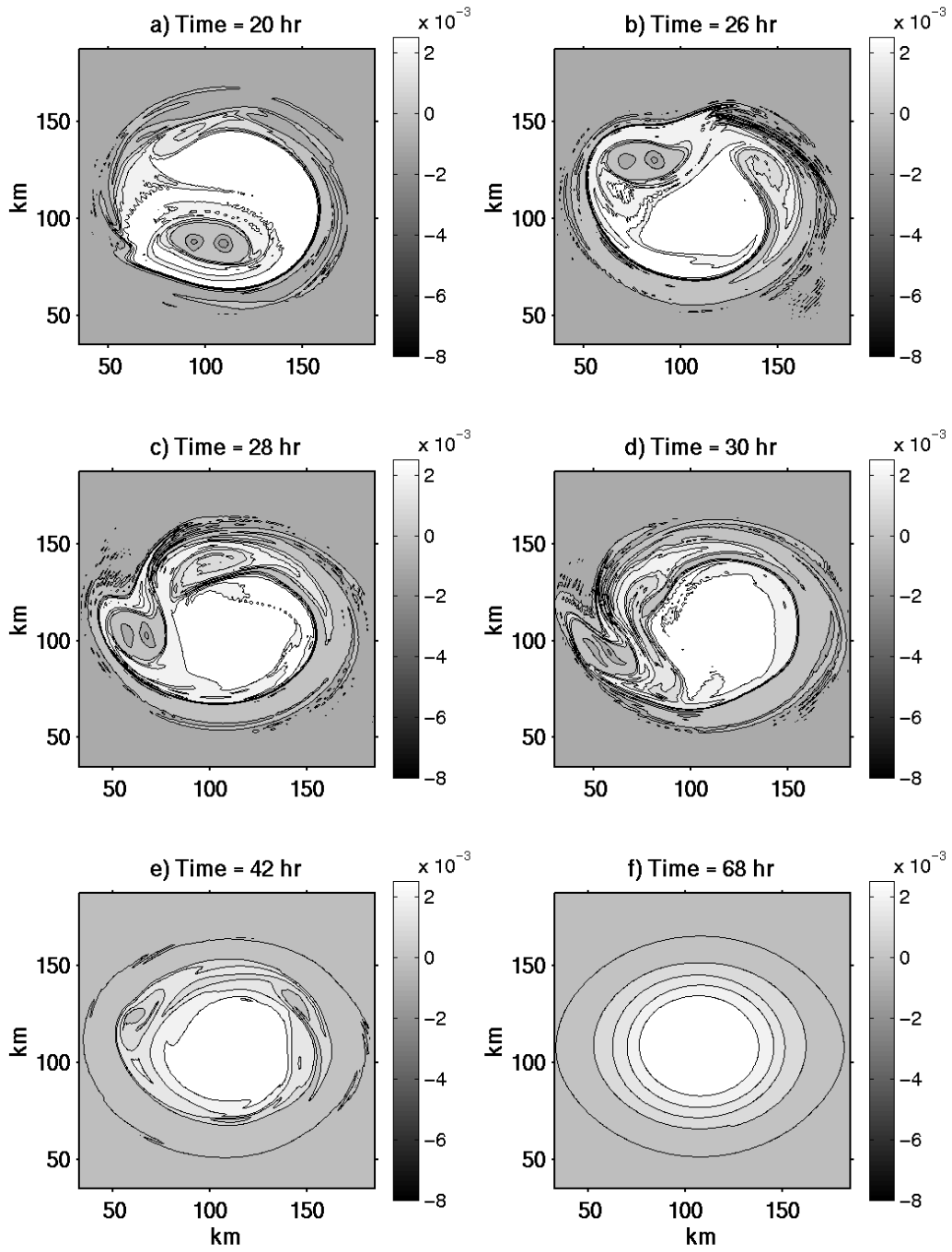
Figure 12. Vorticity fields for Experiment C at a) 20 h, b) 26 h, c) 28 h, d) 30 h, e) 42 h, and f) 68 h.

18
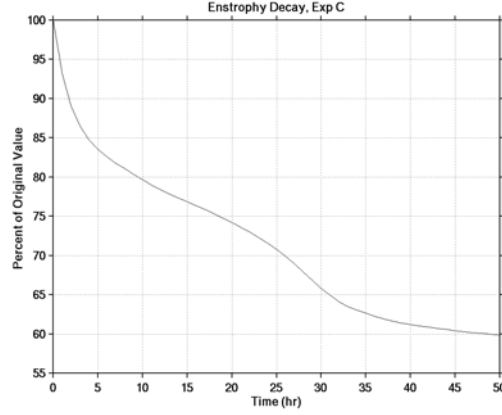
Figure 13. Enstrophy decay for Experiment C.

flow and the asymmetry, the total kinetic energy must be decomposed into the kinetic energy of the mean flow $\overline{KE}$ and the kinetic energy of the contained in the asymmetry KE'.

$$KE = \overline{KE} + KE' \tag{11}$$

In order to form this equation, the wind must first be broken into its mean and perturbation components

$$V = \overline{V} + V' \tag{12}$$

where the V represents the vector wind $V = u\hat{i} + v\hat{j}$. Now in polar coordinates

$$V(r) = \frac{1}{2\pi} \int_0^{2\pi} V d\theta = \overline{u}\hat{i} + \overline{v}\hat{j} \tag{13}$$

But $\overline{u} = -\dfrac{1}{r}\overline{\dfrac{\partial \psi}{\partial \theta}} = 0$, so

$$KE = \frac{1}{A} \int_0^R \int_0^{2\pi} \tfrac{1}{2}(V' + \overline{v}\hat{j}) \cdot (V' + \overline{v}\hat{j}) r d\theta dr \tag{14}$$

where A is the area of integration. Now

$$KE = \frac{1}{2\pi R} \iint \left(\frac{V' \cdot V'}{2} + \frac{\overline{v}^2}{2} + (V' \cdot \hat{j})\overline{v} \right) r d\theta dr \tag{15}$$

19

But $\int_0^{2\pi} (V' \cdot \hat{j}) \bar{v} d\theta = \bar{v} \int_0^{2\pi} (V' \cdot \hat{j}) d\theta = 0$, so

$$KE = \frac{1}{2\pi R} \iint \frac{V' \cdot V'}{2} rd\theta dr + \frac{1}{2\pi R} \iint \frac{\bar{v}^2}{2} rd\theta dr \qquad \textbf{(16)}$$

which is equivalent to equation (11).

For this energy diagnosis, the kinetic energy which would be present in the system if the streamfunction contours were rearranged such that the system is completely symmetric was used as the mean kinetic energy. This was accomplished by first azimuthally averaging the streamfunction over a radius of 108 km from the point of minimum streamfunction, half the width of the domain. Then this azimuthally averaged streamfunction was differentiated to calculate the mean wind speed $\bar{v}$. $\overline{KE}$ bar was calculated using the second term in the right hand side of equation (16).

The total kinetic energy was found by integrating the u and v values in Cartesian coordinates using equation (9) but only over a circle of 108 km radius from the center of the vortex. In this way the total kinetic energy and mean kinetic energy were determined over the same area so that the perturbation kinetic energy could be determined by using equation (11).

Since much of the energy in any system is largely provided through the release of latent heat (Foley, 1995) and the non-divergent barotropic model does not model moisture, the tropical cyclones in this study should not intensify significantly. In fact, the total kinetic energy over the domain is nearly conserved and actually decreases slightly with time due to viscosity, so kinetic energy can only be transferred rather than actually converted from other forms of energy as occurs in non-conservative processes in nature. However, it is the conservative processes being examined. The model can represent those processes (Kossin and Schubert, 2001), so it can model the transfer of kinetic energy between the mean flow and the perturbation that can cause changes in intensity.

The kinetic energy in the asymmetry in Experiment C is plotted as a percentage of the total kinetic energy over time in Figure 14. As the eye was initially off center, the asymmetric kinetic energy started at 8.49 percent and jumped to 14.28 percent as the
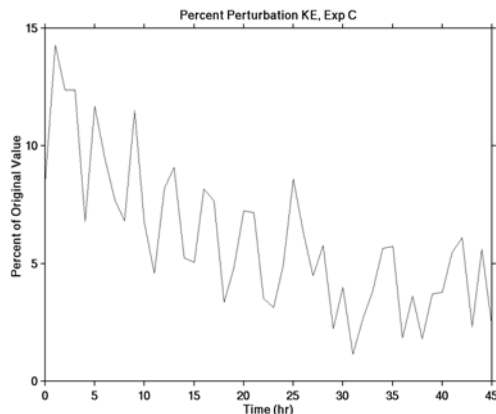
Figure 14. Kinetic energy contained in the asymmetry as a percentage of the total kinetic energy for Experiment C.

mesovortices formed at one hour. Afterward the percentage of kinetic energy contained in the asymmetry oscillated up and down with an amplitude of about four percent, but it generally decreased as the vortex became more and more symmetric. After 30 h, the decreasing trend stopped and perturbation kinetic energy oscillated about a mean value of 3.63 percent. At this point the vortex reached its maximum symmetry. It never became completely symmetric, as the quasi-steady state condition was a tripole with the two satellites unevenly spaced in azimuth about the central pole.

Though this general trend of decreasing then leveling out at 30 h is obvious in Figure 14 and was expected due to the symmetrization of the vorticity pattern, the most striking feature of the kinetic energy plot is the large oscillations about general trend. The period of oscillation varies but its average is 3.5 hours. Figure 15 shows the track of the point of minimum streamfunction, which was used as the center of the vortex for calculating the mean wind profile. This plot shows that the system rotated around a geographic point that was not collocated with the center of the vortex with a period of about 1.7 hours, roughly half the period of oscillations in perturbation kinetic energy. It should be noted that the eye rotation is slower than it would be due to simple advection by the maximum wind. Though this rotation may not be the only factor responsible for the kinetic energy oscillation, it appears to at least play some role. It is also possible that a better method of finding the center might result in a smoother evolution.

21
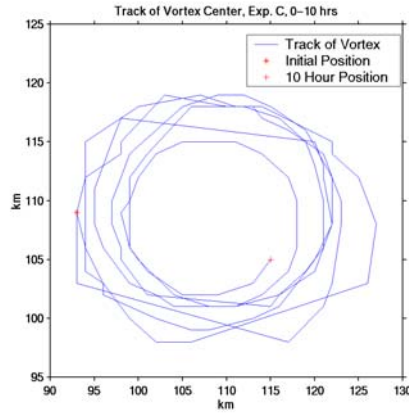
Figure 15. Track of the vortex center for the first ten hours of Experiment C.

Intensity of a tropical cyclone is frequently quantified by the maximum wind speed or minimum sea level pressure. However, the shape of wind profiles can vary significantly, as shown by Weatherford and Gray (1988). Therefore, the average winds over some radial band near the center of the cyclone may well be a better measure of the energy, and probably the destructive power, contained in a tropical cyclone. Weatherford and Gray (1988) defined "strength" of the tropical cyclone as the winds in a band from one to two-and-a-half degrees from the center of the cyclone. Strength and intensity of a hurricane are not always closely correlated. In fact, Weatherford and Gray cite the case of Supertyphoon Wynne in which the central pressure fell 59 mb in twelve hours with no change in strength. This study considers the wind profiles closer to the center, typically in the innermost 70 km. Figure 16 shows that the maximum wind speed in Experiment C decreased by 11.8 percent during the model run. However, this maximum
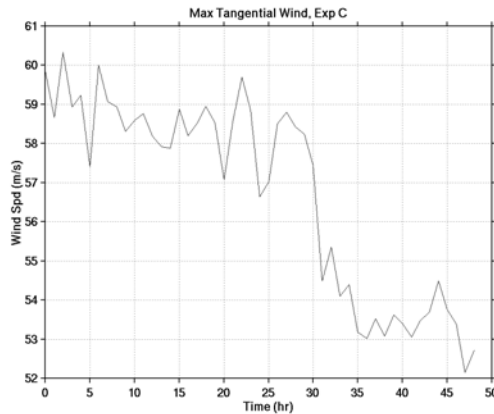
Figure 16. Maximum tangential wind speed for Experiment C.

22

wind, which was initially 59.8 m/s, covered a very small area. The maximum azimuthally averaged wind speed actually increased from 43.5 m/s to 46.5 m/s during the first 24 hours and remained relatively constant thereafter. An examination of Figure 17 will show that the azimuthally averaged wind speed over the entire band from the center out to about 70 km increased as the vortex became more symmetric.
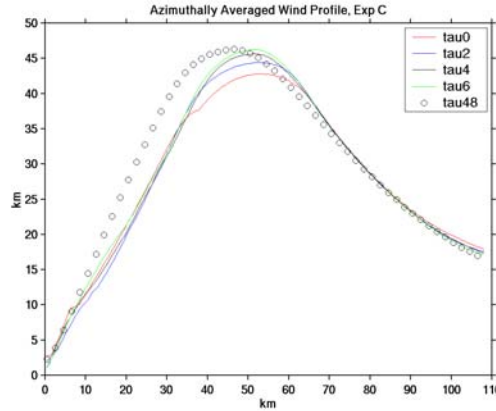
Figure 17. Azimuthally averaged wind profiles for Experiment C at zero, two, four, six, and 48 hours.

The kinetic energy evolution of Experiment B, depicted by Figure 18, proceeded similarly to Experiment C with a slight initial increase as the mesovortices formed and increased asymmetry, followed a decrease in the perturbation kinetic energy. This decrease stops with *KE*' oscillating about a mean of around five percent from hours five
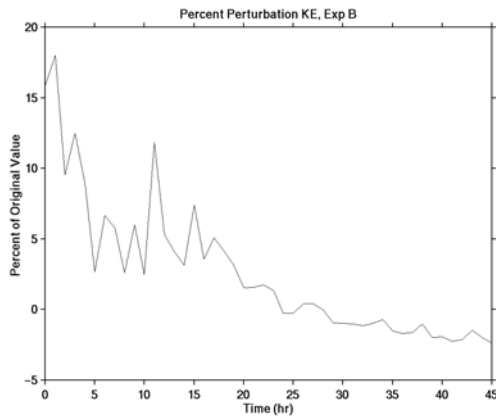
Figure 18. Kinetic energy contained in the asymmetry as a percentage of the total kinetic energy for Experiment B.

through nineteen and again decaying afterward. During this final decay, the amplitude of the oscillations also decayed. The percent perturbation kinetic energy was actually a small negative value after 27 h, which was obviously caused by an error of some type. A full discussion of the reasons for this negative result is given in section III.B.3 below. As in Experiment C, the maximum wind speed decreased, but the maximum azimuthally averaged wind speed increased as shown in Figure 19. This figure shows that the average winds in the inner 70 km band also increased as the vortex was symmetrized.
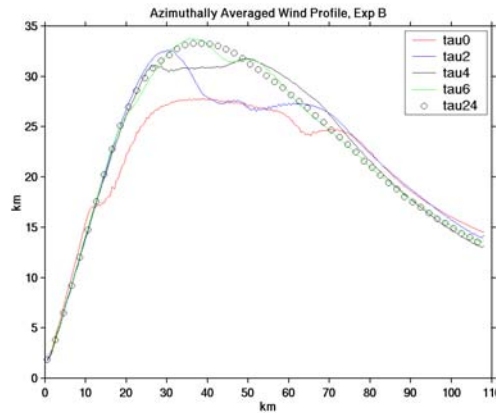
Figure 19. Azimuthally averaged wind profiles for Experiment B at zero, two, four, six, and 24 h.
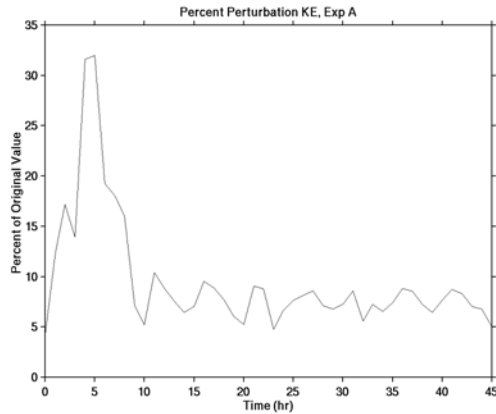
Figure 20. Kinetic energy contained in the asymmetry as a percentage of the total kinetic energy for Experiment A.

Perturbation kinetic energy increased significantly during the first five hours of integration in the initially symmetric eye case, Experiment A, as the vorticity pattern was

broken up and became extremely disorganized, as shown in Figure 20. The energy that was transferred from the mean flow to the asymmetry, 32 percent of the total KE, was very quickly transferred back to the mean flow as symmetrization occurred. The perturbation kinetic energy oscillated about a mean of 7.5 percent at all times after ten hours. The period of this oscillation was quite irregular. An examination of the center of minimum streamfunction location showed that its movement was highly erratic, rather than the regular inward-spiraling path followed in Experiment C. Figure 21 shows that a massive drop in the maximum azimuthally averaged wind speed as violent mixing tore the cyclone structure apart in the first five hours. As in the first two cases, the wind speeds increased afterward as the vortex again became symmetric, but the final maximum was still lower than the initial value.
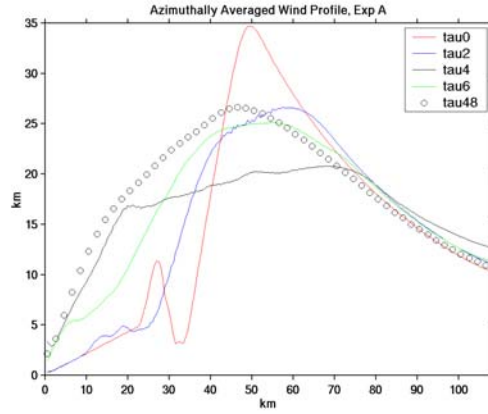
Figure 21. Azimuthally averaged wind profiles for Experiment B at zero, two, four, six, and 24 h.

B.   OFFSET VORTICITY MONOPOLE EXPERIMENTS

1.   Initial Conditions

The initial conditions for the offset vorticity monopole experiments, also taken from PKS, are an idealized representation of a tropical storm with an offset area of intense convection. The initial vorticity field is a circular region of radius a, centered at $x = x_C$, $y = y_C$. The maximum value of vorticity is not located at the center of the circle, but rather at $x = x_M$, $y = y_C$. Vorticity decreases monotonically in all directions

from this maximum point. As in the offset eye experiments, ζ_e is chosen such that the average vorticity over the entire domain equals zero.

Mathematically, the initial condition is given by

$$\zeta(x,y,0) = \zeta_e + \hat{\zeta}\begin{cases} S\left(1 - \dfrac{\sqrt{(x-x_M)^2 + (y-y_C)^2}}{d}\right), & \left[(x-x_C)^2 + (y-y_C)^2\right] \le a^2 \\ 0, & \left[(x-x_C)^2 + (y-y_C)^2\right] \ge a^2 \end{cases}$$

where

$$S(r) = \exp\left[-\frac{\kappa}{r}\exp\left(\frac{1}{r-1}\right)\right]$$

The distance value d is calculated by first finding

$$A = \arctan\left(\frac{|y - y_C|}{x - x_M}\right)$$

The value for A is then substituted into

$$B = \arcsin\left(\frac{x_C - x_M}{a}\sin A\right)$$

Finally, d is determined using A and B.

$$d = a\frac{\sin(A + B)}{\sin A}$$

The peakedness of the field is determined by the parameter κ. In these experiments the vorticity is quite sharply peaked with $\kappa = \frac{1}{2}\exp(2)\ln(2) \approx 2.5609$. This steep vorticity gradient necessitates the use of viscosity in the integration of the model to damp the cascade of vorticity to smaller and smaller scales and producing excessively noisy results.

For the control run, Experiment D, the maximum vorticity was located at the center of the vortex. Experiments E and F were run with very offset and slightly offset monopoles respectively. All parameters used in the equations above, along with the distance maximum vorticity is offset, $x_C - x_M$, are listed in Table 2. The initial vorticity

26
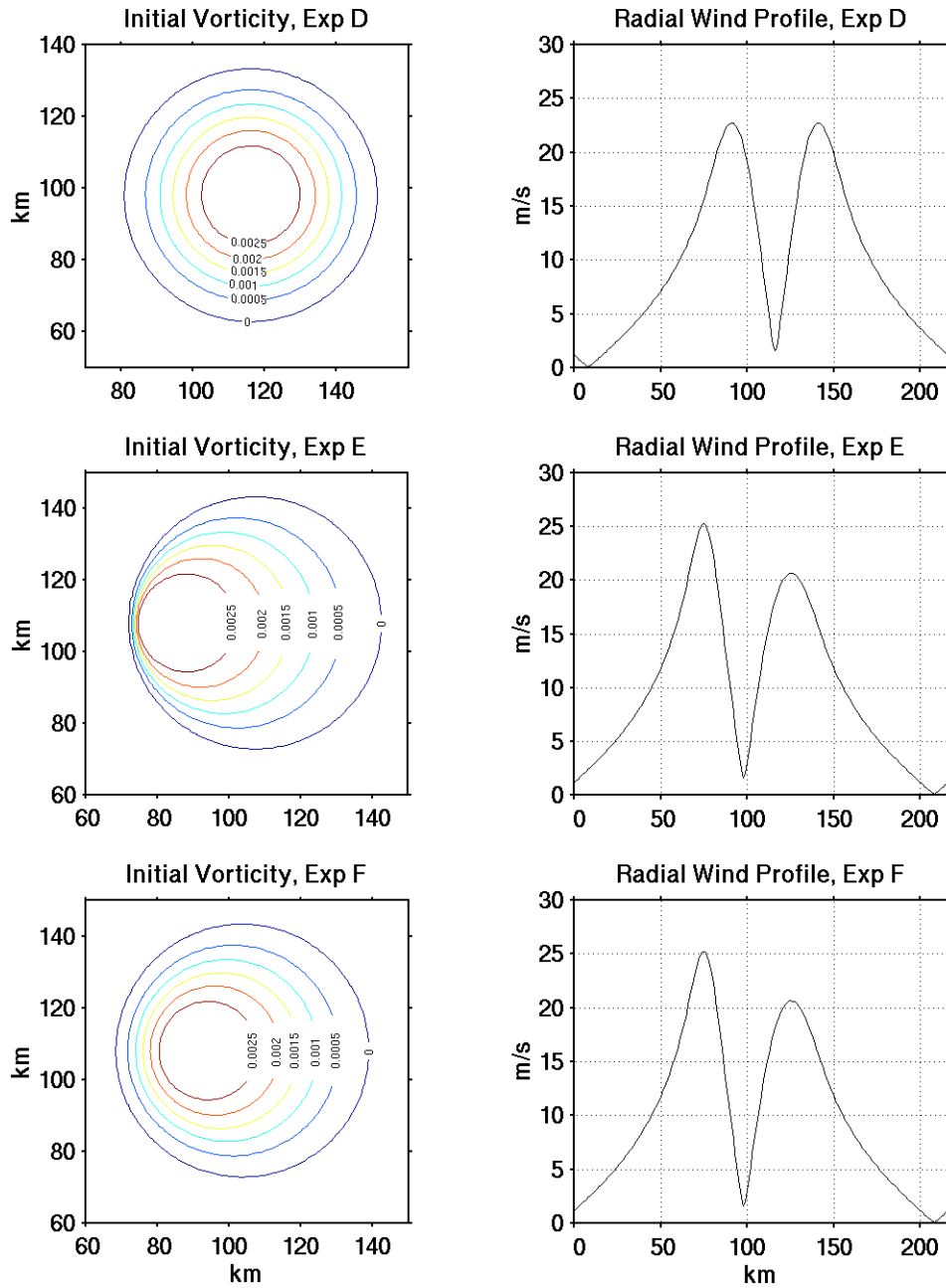
Figure 22. Initial vorticity field and wind profile for all monopole experiments. The wind profile shown is taken east-west across the center of the vortex.

field and a corresponding profile of winds across the vortex is shown for each of these experiments in Figure 22.

Exp.	a	x_C	x_M	$x_C - x_M$	$\hat{\zeta}$	ζ_e	PKS Exp.
	(km)	(km)	(km)	(km)	$(\times10^{-5}\text{s}^{-1})$	$(\times10^{-5}\text{s}^{-1})$	
D	45	116.1	116.1	0	300	-11.4	N/A
E	45	116.1	76.1	40	300	-11.4	A
F	45	108.1	88.1	20	300	-11.4	C

Table 2.   Initial condition parameters for offset monopole experiments.

2.   Vorticity Structure Evolution

The vorticity evolution of the monopole experiments was also similar to that of

PKS. The sign of $\dfrac{\partial \zeta}{\partial r}$ does not change, so the necessary condition for barotropic
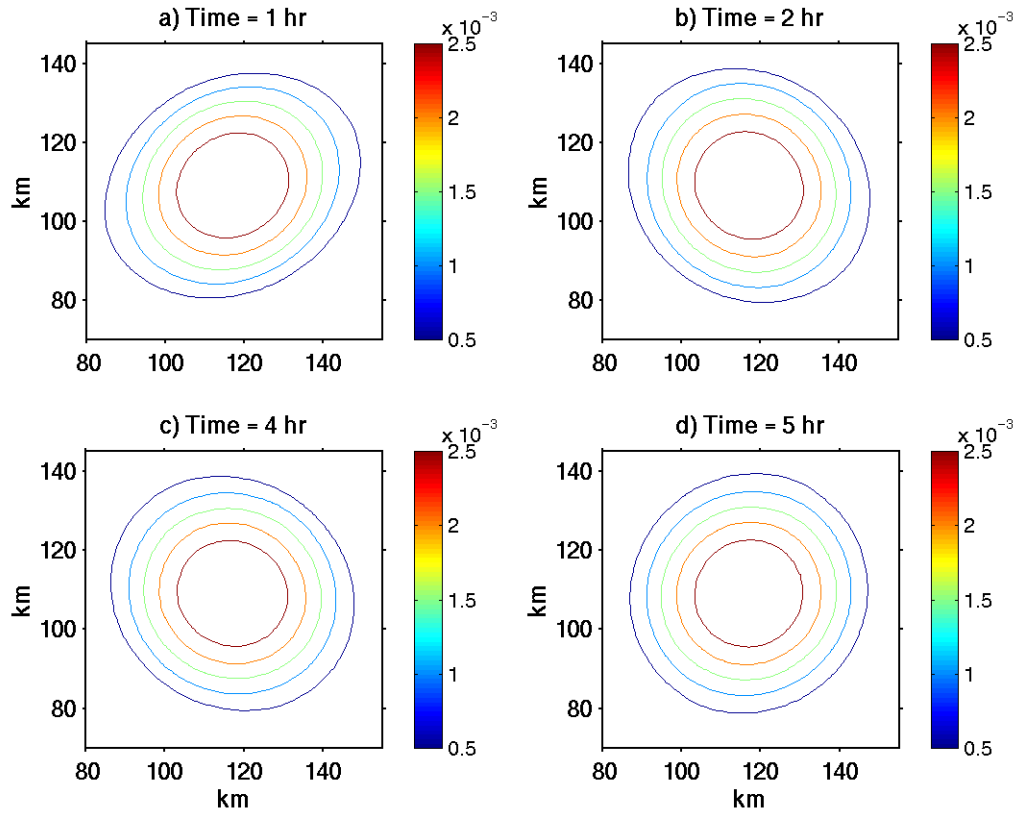
Figure 23. Vorticity fields for Experiment D at a) one hour, b) two hours, c) three hours, and d) five hours.

instability is not met, though $\dfrac{\partial \zeta}{\partial r}$ does change from negative values to zero at a radius of about 45 km from the center of the vortex. Since the vortex cannot be barotropically unstable, the vortex structure does not break apart in violent mixing as in the eye cases. Weaker mixing does occur, however, mostly due to the formation and break up of spiral bands and a possibility for weak barotropic instability develops in later hours as lower vorticity fluid is surrounded by higher vorticity spiral bands.

The vorticity evolution of Experiment D is shown in Figures 23 and 24. The vortex, which was an initially symmetric monopolar structure, become very slightly elliptical almost immediately and rotated cyclonically with a period of 8.37 h. This period equates to a 5.4 m/s speed of movement around the radius of maximum winds. Since the maximum wind is 26.5 m/s, there must be wave propagation upstream at 21.1 m/s to result in this rotation. This is in the correct sense for a vortex Rossby wave. This
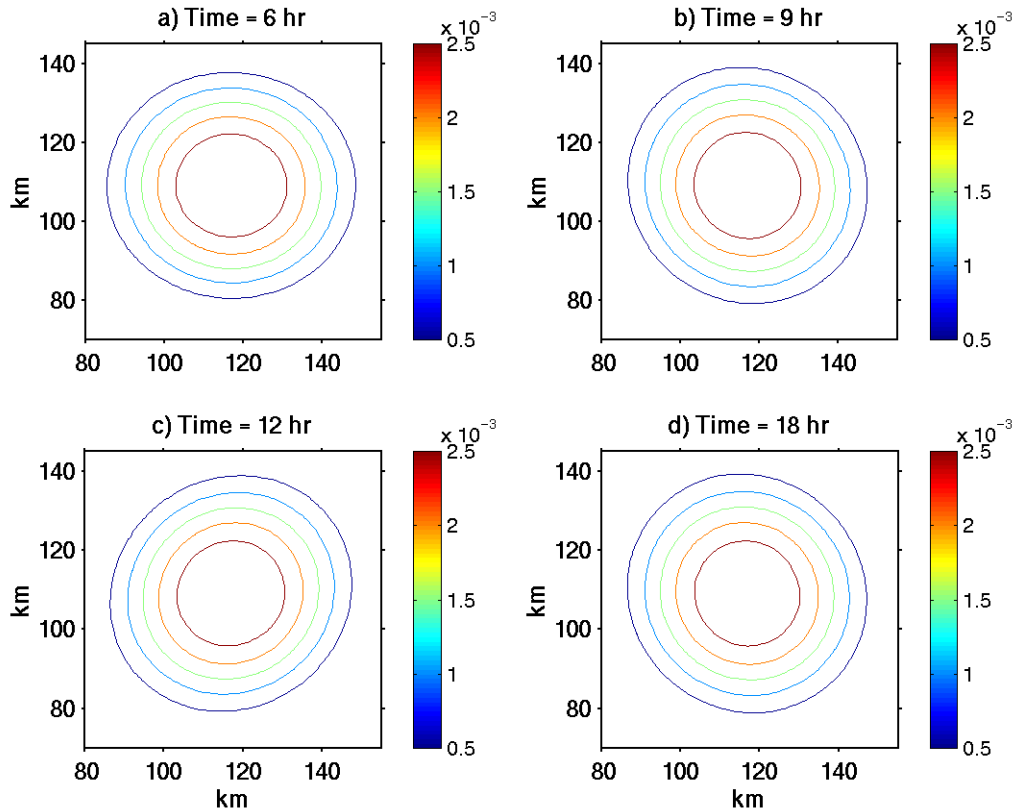
Figure 24. Vorticity fields for Experiment D at a) six hours, b) nine hours, c) twelve hours, and d) eighteen hours.

rotation continues through hour five as shown in Figures 23a though 23d and then the vortex is circular again at six hours. At nine hours, the vortex again becomes elliptical, but almost imperceptibly so. The vortex is completely symmetric and circular at eighteen hours and remains so for the remainder of the 50 hour model run. As there is little to no mixing in this case, the enstrophy decays at a slow and nearly constant rate through the entire model run. The decrease in enstrophy over the entire 50 hours is only 6.5 percent.

Experiment E was an offset monopole with the point of maximum vorticity very near the western edge of the vortex. Figures 25 and 26 depict the development of the vorticity in this very asymmetric, yet barotropically stable, case. Though violent mixing as in the off center eye experiments never occurs, axisymmetrization and some mixing through development of a spiral band begin in the first hour. By hour two, the band had

Figure 25. Vorticity fields for Experiment E at a) one hour, b) two hours, c) four hours, and d) six hours.

Figure 26. Vorticity fields for Experiment E at a) eight hours, b) nine hours, c) fourteen hours, and d) 27 hours.

grown into a thin filament extending about a quarter of the distance around the vortex and the inner contours of vorticity were also distorted outward toward lower vorticity. The band had grown half way around the vortex at four hours and the monopole had moved to a location near the center, though none of the contours were circular. At eight hours, the band enclosed a thin band of negative vorticity and its end broke off mixing the positive vorticity outward. By fourteen hours, the vortex was essentially symmetric but the contours were not yet quite circular and the completely symmetric and circular equilibrium state was reached at 22 h. The mixing through spiral band formation and break up was accompanied by an enstrophy cascade of six percent in the first eleven hours of integration. Afterward the enstrophy decay continued at a slow constant rate for a total decrease of eleven percent in 50 hours.

Experiment F was initialized with the same maximum vorticity as Experiment E, but was offset by 20 km instead of the 40 km used in Experiment E. This experiment developed similarly to Experiment E, but the spiral band developed later and, since the field was initially less asymmetric, the final symmetric state was reached more quickly. The vorticity series for this experiment is shown in Figures 27 and 28. At one hour all contours remained quite smooth, but the entire structure had become elliptical and rotated cyclonically. The center of the monopole had also moved closer to the geographic center of the vortex. A large smooth bulge developed along the outer edge of the positive vorticity region at two hours. The spiral band began to develop at hour four, three hours later than in Experiment E. The band grew and its end began to break off at six hours, mixing positive vorticity into the outer region. In the next hour the band continued to grow and break off. The next two contours also formed bands extending into lower vorticity, mixing positive vorticity outward from the center. At nine hours, the bands
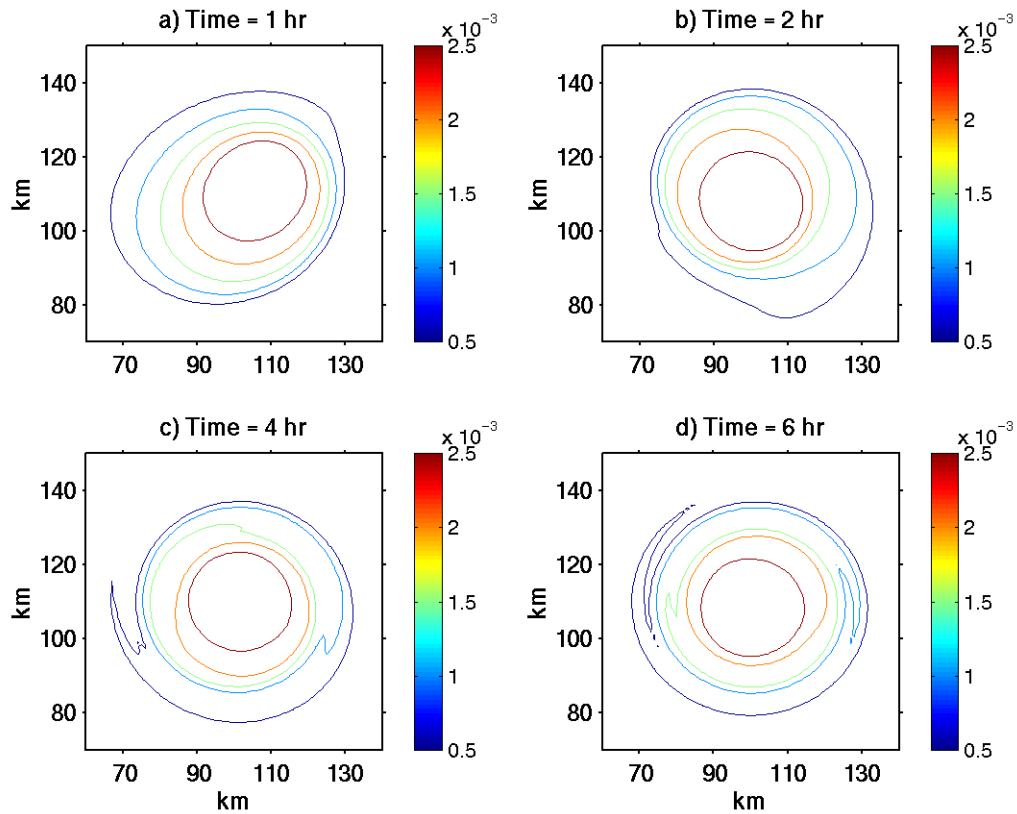
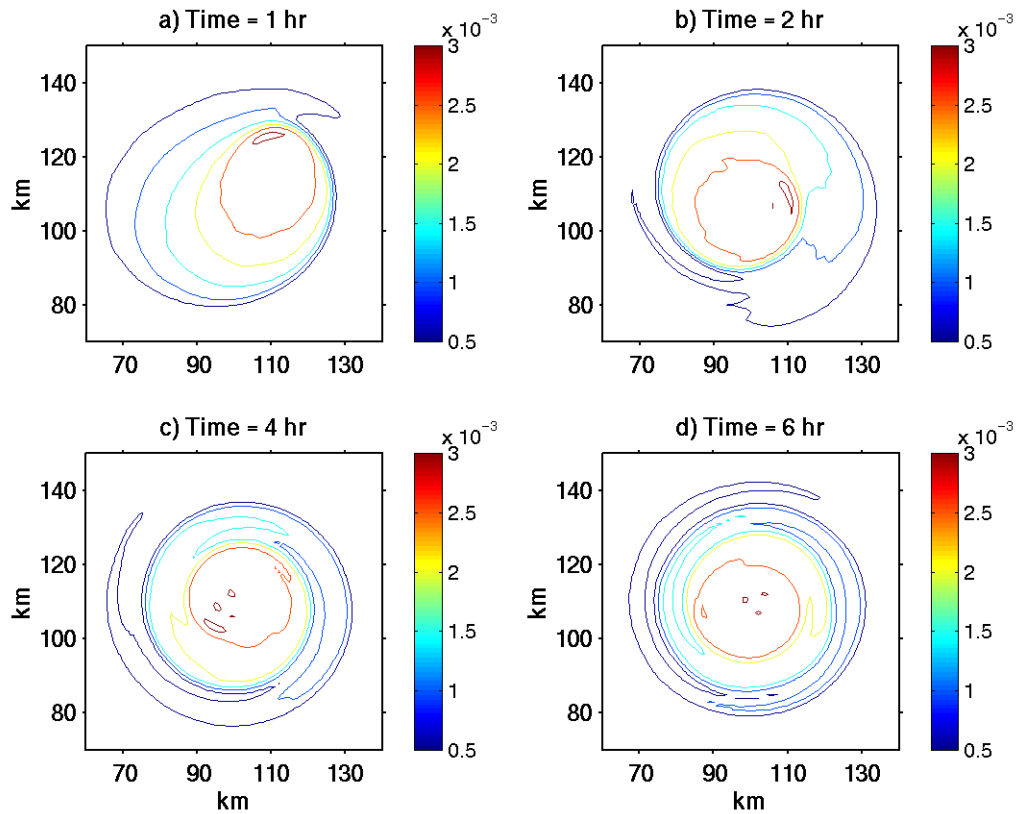Figure 27. Vorticity fields for Experiment F at a) one hour, b) two hours, c) four hours, and d) six hours.

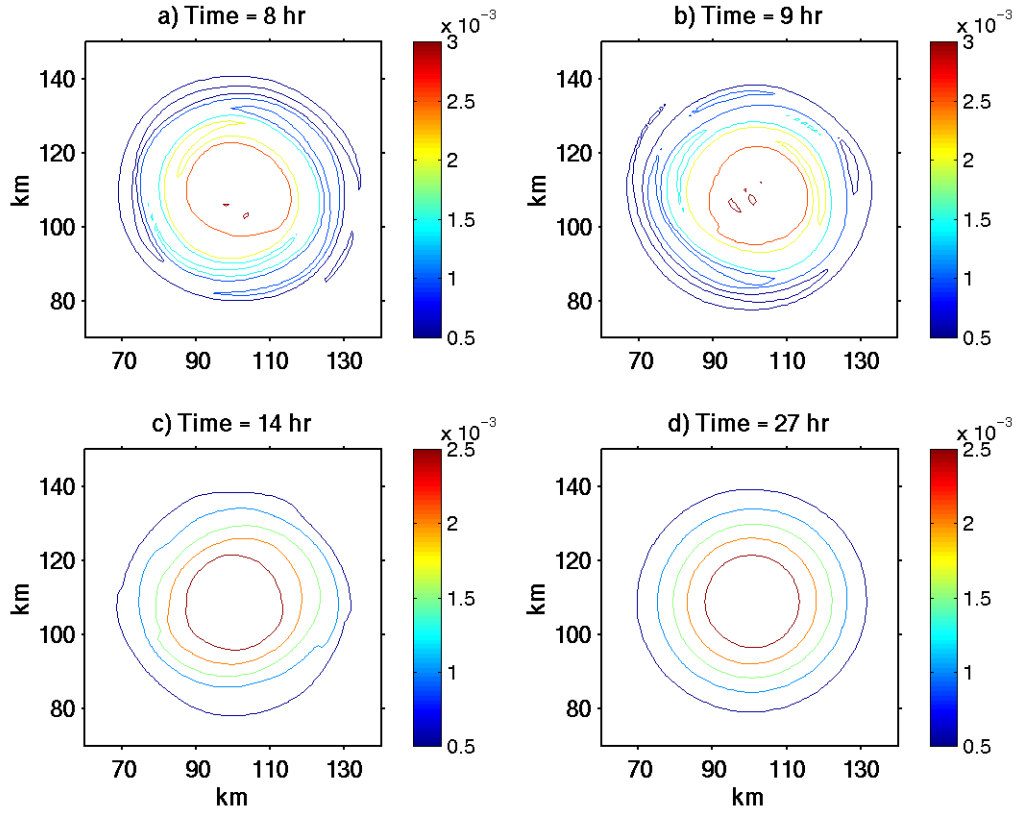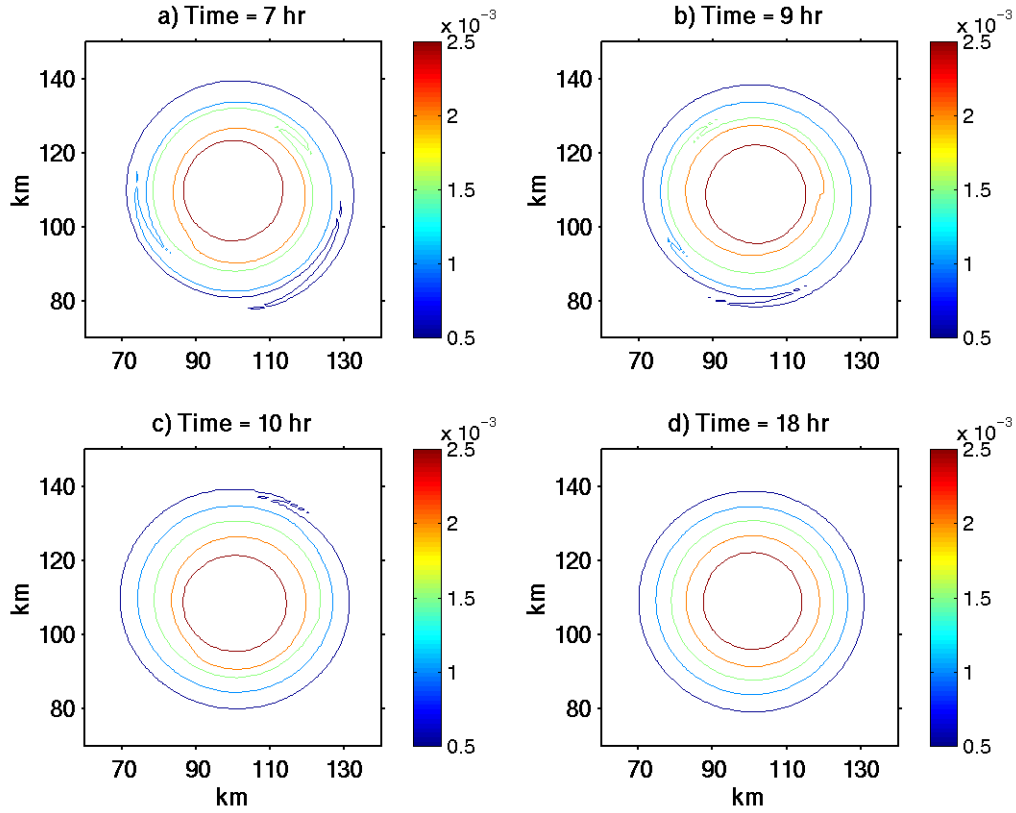Figure 28. Vorticity fields for Experiment F at a) seven hours, b) nine hours, c) ten hours, and d) eighteen hours.

began to shrink, forcing the structure toward a circular shape. After ten hours, only a small remnant of the outer band remained and the inner bands had disappeared altogether. After eighteen hours, the completely circular equilibrium state was reached, four hours earlier than in Experiment E. As should be expected by the band formation and mixing described above, the sharpest enstrophy cascade occurred between hours two and ten, though the decay during this period was only 2.5 percent. After hour twelve, a gradual constant decay continued through the end of the 50 hour model run.

3.   Wind Profile Evolution and Kinetic Energy Transfers

The offset monopole cases were not unstable and the azimuthally averaged wind profiles did not change as significantly with time as the offset eye cases did. A much smaller percentage of kinetic energy was contained in the asymmetries in the monopole

experiments than in the offset eye cases. However, small energy transfers between the asymmetries and the mean flow did occur.

Figure 29 shows the kinetic energy contained by the asymmetry as a percentage of the total kinetic energy through 45 hours of model integration for Experiment E, which is typical of these cases. As a large bulge, which will later become the spiral band, forms on one side of the vortex at one hour, the system is actually more asymmetric than it began and the kinetic energy in the asymmetry actually increases slightly. Later the fluid contained in this bulge wraps around the vortex as a spiral band and the area of maximum vorticity moves toward the geographic center of the vortex, increasing symmetry and thereby decreasing the kinetic energy contained in the asymmetry. The perturbation kinetic energy decreases until hour five when the central monopole is slightly offset to the side of the vortex where the spiral band lies. Even though the vortex was not yet circular, its structure was such that the arrangement of kinetic energy was quite symmetric.

After the first five hours, the percent kinetic energy oscillates with an eleven hour period between values of approximately 0.3 percent and –0.9 percent. Obviously, the mean kinetic energy cannot be greater than the total kinetic energy, which would be required for perturbation kinetic energy to be negative. The most likely reason for this occurrence lies with the wind calculation method. The wind speeds used to calculate the total kinetic energy were determined from streamfunction by the model using a spectral
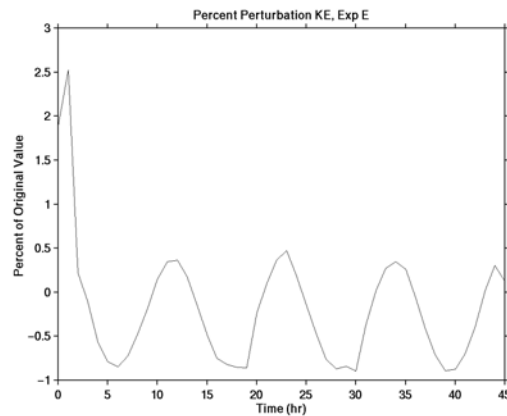

Figure 29. Kinetic energy contained in the asymmetry as a percentage of the total kinetic energy for Experiment E.

34

method over the square domain. The mean wind speed used in the mean kinetic energy calculation was determined from the azimuthally averaged streamfunction by finite differencing. The difference in differentiation methods results in a very small difference in the wind speeds calculated even if the streamfunctions are exactly the same. Since the mean wind speed is quite low, the difference in wind speed needed to produce a kinetic energy perturbation of –0.9 percent vice zero percent is only 0.04 m/s. The mean wind speed over the domain was near 8.5 m/s at the times when these negative kinetic energy values occurred. The difference of 0.9 percent in kinetic energy could occur by using 8.46 m/s instead of 8.5 m/s as the mean wind speed. While this difference would be unnoticed in experiments with higher mean wind speeds, it results in a negative perturbation kinetic energy calculation here. It is also possible that some error was introduced due to corners in the domain. Even though only the winds within the 108 km radius used in the kinetic energy calculation, the wind field was calculated over the entire square domain.

This problem, however, can only result in a systematic error which should be a constant percent of the kinetic energy value. While it can cause the erroneous negative values to occur, it is not responsible for the sinusoidal oscillation in the perturbation kinetic energy. Figure 30 shows that, while the vortex appears to have become completely circular and symmetric, fluctuations in the wind speed did occur. In these plots, the azimuthally averaged wind profiles for the times of the local maximum and local minimum perturbation kinetic energy are plotted together. The plots on the left side of the figure show that, while much of the profile remains unchanged, the wind speed in the outer 20 km of the area examined was consistently as much 0.5 m/s higher when the minimum perturbation kinetic energy occurred than when the maximum occurred. The plots on the right hand side of the figure show the same profile, zoomed in on the area around the radius of maximum wind in the vortex. The wind at times when minima of perturbation kinetic energy occurred was 0.1 to 0.2 m/s higher than at times of the maxima in this region. These wind fluctuations are consistent with the oscillations in perturbation kinetic energy, as higher mean wind leads to higher mean kinetic energy and therefore lower perturbation kinetic energy at the times when the minima occur. The
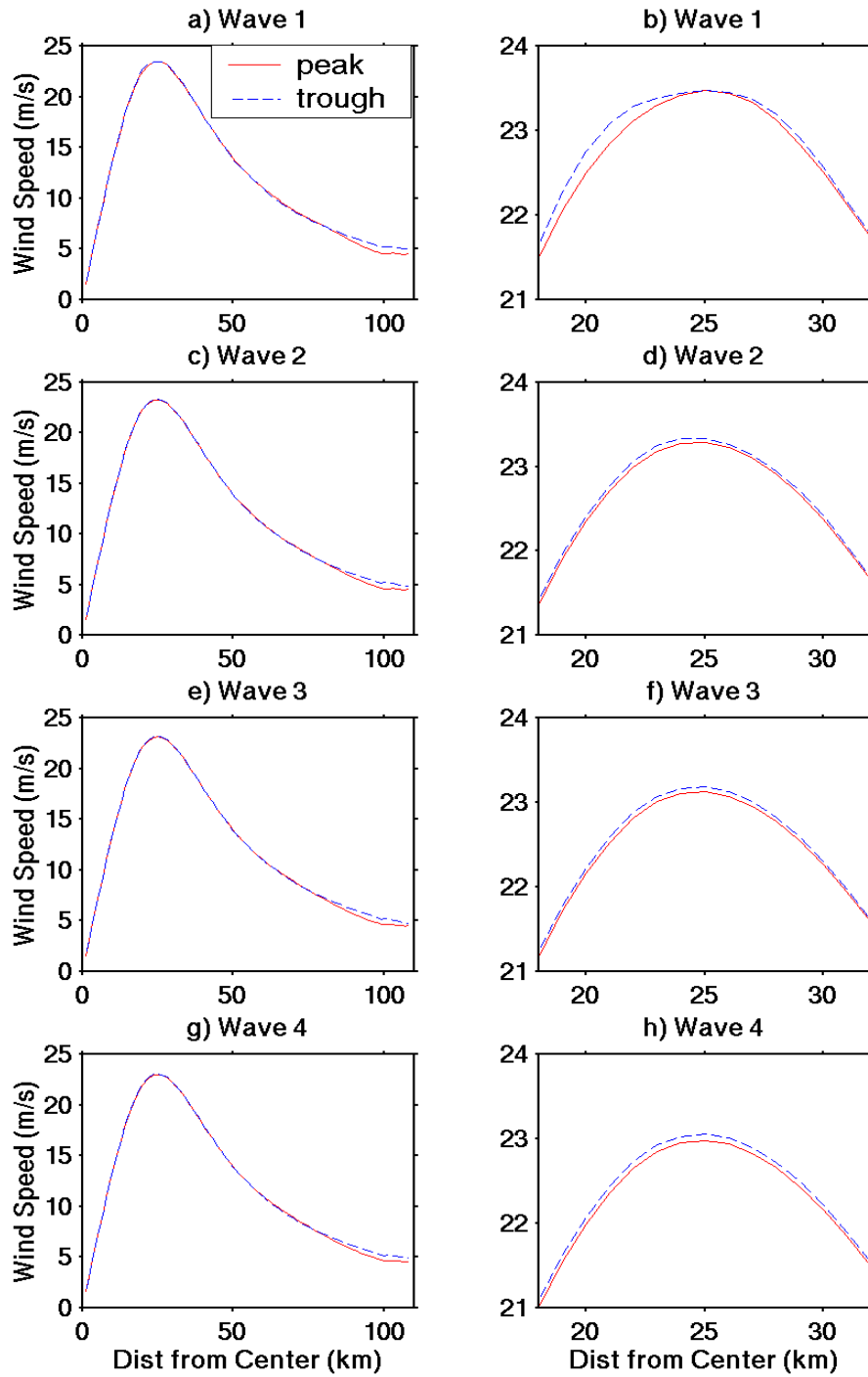
Figure 30. Azimuthally averaged wind profiles for Experiment E at the times of the local maxima and minima for each wavelength of KE' oscillation. b), d), f), and h) show the zoomed in area around the radius of maximum winds.

reason for these oscillations in wind speed could not be determined for certain, but possible mechanisms were explored. First, vortex Rossby wave propagation such as that in Typhoon Herb (Kuo, et. al., 1999) were considered. If the vorticity in the innermost six km in Figure 31 (azimuthally averaged vorticity profile for Experiment E at six hours, when the fluctuations begin) is considered to be constant, then the linear vorticity wave phase speed can be calculated by

$$c = V_{max}\left(1 - \frac{1}{m}\right)$$

where V_{max} is the maximum wind speed and m is wavenumber (Thomson, 1880; Lamb, 1932; and Kuo, et. al., 1999). The vorticity in this region is not actually constant, but decreases very slightly so this assumption is reasonable. A wavenumber 5 vortex Rossby wave would then have an upstream phase speed of 20.58 m/s, resulting in a cyclonic rotation with an 11.02 hour period, which matches closely with the 11 hour period in the fluction in wind speed. However, this is unlikely to be the mechanism causing the fluctuations, as the winds around the radius of maximum wind and the winds in the outer region of the vortex vacillate with the same period. Further, the vorticity gradient in the outer 20 km is zero, or very near zero, so that region provide no medium for a vorticity wave to propagate upon.
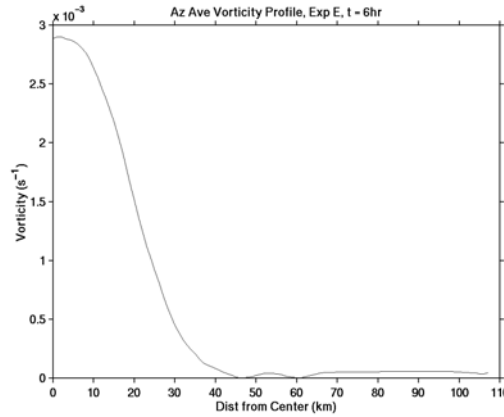
Figure 31. Azimuthally averaged vorticity profile for Experiment E at six hours.

The kinetic energy evolution of the other two cases proceeded very similarly to Experiment E. The peak in perturbation kinetic energy for Experiment F only reached

1.7 percent, vice the 2.5 percent for Experiment E, which is reasonable as the vortex was initially less asymmetric. Both this case and the initially symmetric Experiment D resulted in a sinusoidally oscillating final state in kinetic energy with approximately the same amplitude and period as in Experiment E.

Though the offset monopole cases showed a transfer of kinetic energy from the asymmetry to the mean flow, the magnitude was much less than in the off center eye cases. Modification of the azimuthally averaged wind profiles, shown in Figure 32, by the axisymmetrization process occurred in a much narrower band and was less significant than in the eye experiments. These effects illustrate that for these cases, which would typically occur during the tropical storm phase of the tropical cyclone life cycle, axisymmetrization does not have a significant effect on the intensity or strength of a tropical cyclone.
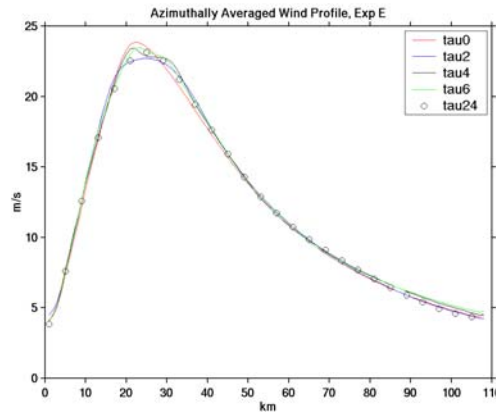
Figure 32. Azimuthally averaged wind profiles for Experiment E at zero, two, four, six, and 24 hours.

C.   FURTHER EXPERIMENTS

Several further experiments were conducted to study other possible effects on the development of the systems. All experiments described in previous section were integrated using an f-plane model. Various initial conditions from these experiments were also modeled with the inclusion of beta. Since the outer wind profile of the vortices studied does not decrease to zero inside the model domain, one experiment was run on a larger domain to ensure that the wind profiles produced in the experiment were not being contaminated by the boundaries of the model. Two additional experiments demonstrated

the need for friction. Finally, one experiment was studied in much finer temporal resolution to determine the details of initial mesovortex formation. A brief summary of all further experiments is provided in table 3 below.

Exp.	Description of Initial Conditions
G	Initially symmetric monopole, same as Experiment D. Integrated on beta plane.
H	Monopole initially offset 40 km, same as Experiment E. Integrated on beta plane.
I	Medium sized offset eye, same as Experiment B. Integrated on beta plane.
J	Initially symmetric monopole with structure the same as Experiment D, but with all dimensions of both the vortex and the domain twice as large. Integrated on beta plane.
K	Same initial conditions as Experiment D, but with domain 648x648 km (three times as large). Integrated on *f*-plane.
L	Same initial condition as Experiment D, but integrated on *f*-plane with no friction.
M	Same initial conditions used by Kuo, et. al. (1999) to simulate Typhoon Herb. Integrated on *f*-plane with no friction.
N	Medium sized offset eye, same as Experiment B, but integrated on f-plane with output every five minutes during first hour.

Table 3.   Summary of initial conditions for all further experiments.

1.   Beta Plane Experiments

Since the beta effect was found to be important at relatively small scales in a study of the interaction between monsoon circulation and tropical disturbances (Kuo, et. al., 2001), several experiments were conducted to determine whether the beta effect would play any significant role in the development of the vortices studied in this research. The same model was used for these experiments, except that the barotropic vorticity equation was modified to include the beta term as described in Section II. A constant value of $\beta = 2.205 \times 10^{-11} m^{-1} s^{-1}$ was used for all beta plane experiments, which places the center of the vortex at 15˚ latitude.

Experiment G was run with the same initial conditions as Experiment D, but was integrated using the beta plane instead of the *f*-plane. The structure of the vortex evolved exactly as it did on the *f*-plane, but beta effect propagation moved the vortex 7.5 km

westward in 72 h, resulting in a propagation speed of only 0.03m/s. This very slow westward movement is consistent with previous research that shows that beta effect propagation (BEP) speed is a function of the radius of the vortex and the slope of the outer portion of the wind speed profile (Chan and Williams, 1987 and Fiorino and Elsberry, 1989). Since this vortex has a very small radius and the wind speed decreases very sharply outside the radius of maximum winds, a very slow westward movement is reasonable. Figure 33 shows the vortex at 12, 24, 36, and 48 h with the *f*-plane and beta plane results overlaid to demonstrate the similarity of the structure and show this slow westward drift. The azimuthally averaged wind profiles and the kinetic energy time series (not shown) were exactly the same as those of the *f*-plane case.
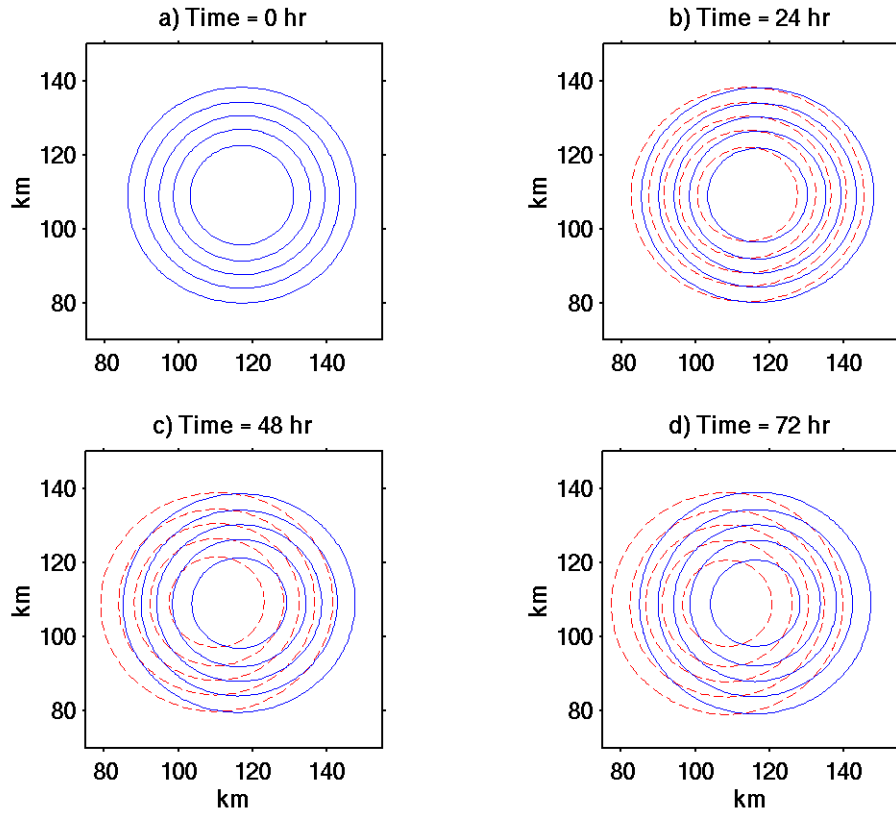
Figure 33. Vorticity fields for Experiment G at a) 0 h, b) 24 h, c) 48 h, and d) 72 h. The *f*-plane case is plotted in solid blue lines and the beta plane case in dashed red lines.
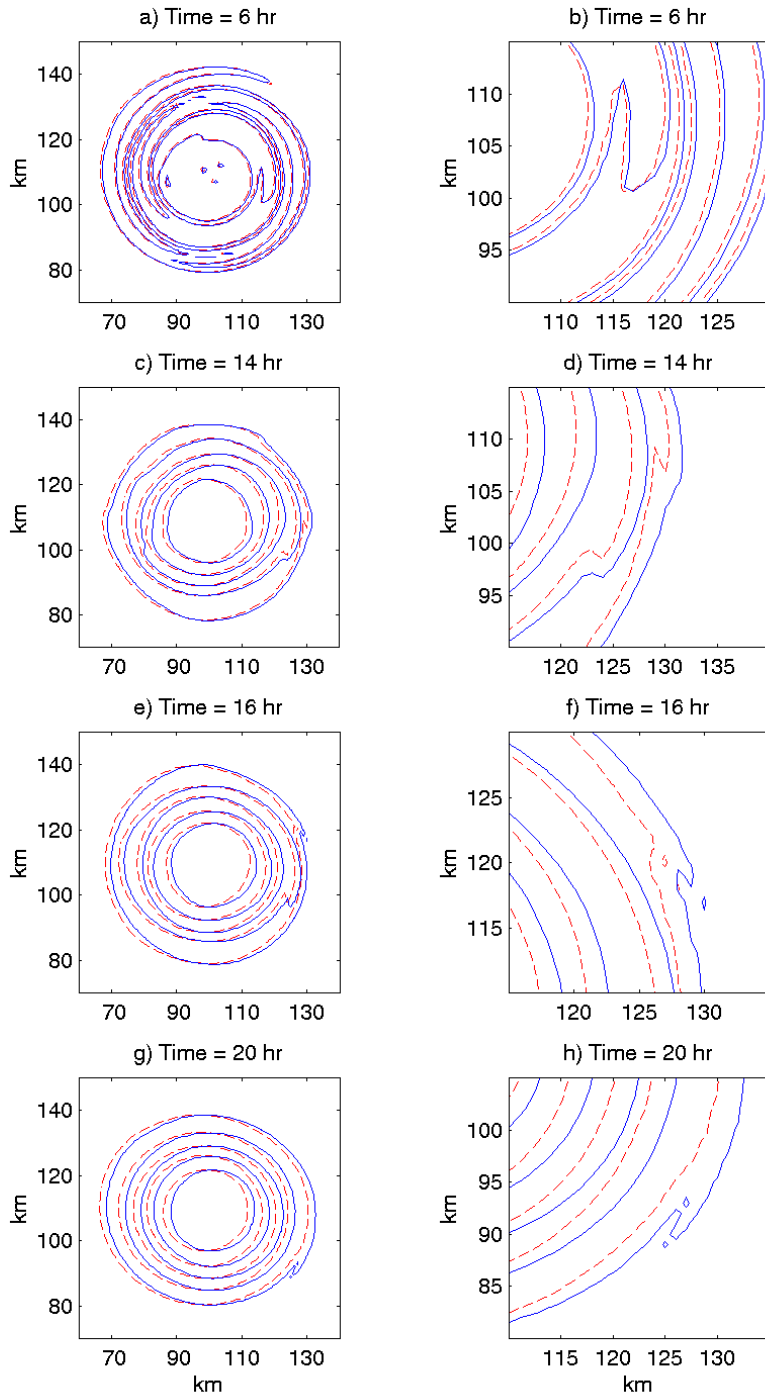
Figure 34. Vorticity fields for Experiment H at a) 6 h, c) 14 h, e) 16 h, and g) 20 h. Panels b), d), f), and h) are zoomed in on perturbation areas. The *f*-plane case is plotted in solid blue lines and the beta plane case in dashed red lines.
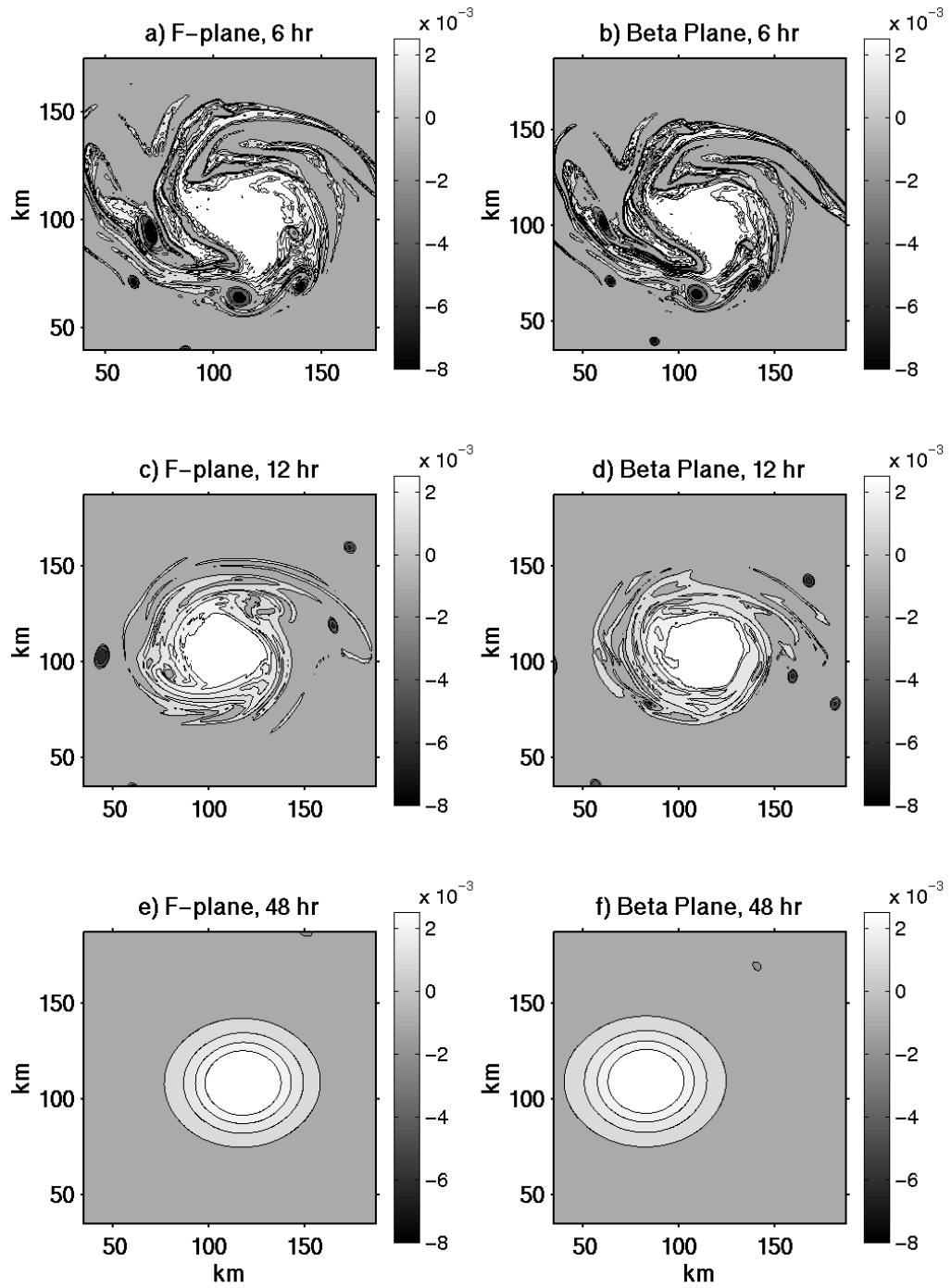
Figure 35. Vorticity fields for Experiment I at a) 6 h (*f*-plane), b) 6 h (beta plane), c) 12 h (*f*-plane), d) 12 h (beta plane), e) 48 h (*f*-plane), and f) 48 h (beta plane).

Experiment H was the integration of the very offset monopole, Experiment E, on the beta plane. In the early hours, the beta plane and *f*-plane results are exactly the same. By hour six, the slight westward movement of the vortex in the beta plane case is clearly evident, but perturbations in the vorticity pattern are still virtually identical as illustrated by Figure 34a. Between fourteen and 20 h, small differences in the *f*-plane and beta plane cases exist as shown in Figure 34b, 34c, and 34d. Still these differences are only in the fine structure of perturbations in the pattern. The overall pattern is still the same except that the beta plane case is shifted toward the west. By tau24, the vortex was essentially axisymmetric and only fine smoothing of the contours occurred after this point. The beta plane and *f*-plane patterns were again identical and remained so through all subsequent times. As the vorticity fields were so similar, the resulting azimuthally averaged wind profiles and kinetic energy time series were again identical.

The medium offset eye was also integrated on the beta plane. This case, Experiment I, used the same initial conditions as Experiment B. This experiment proceeded exactly as Experiment B except for the slight westward drift described above in Experiments G and H. Since the vorticity pattern is much more complex than in the monopole cases, overlaying vorticity from *f*-plane and beta-plane cases together cannot be easily read so Figure 35 shows the vorticity at selected times from the *f*-plane and beta
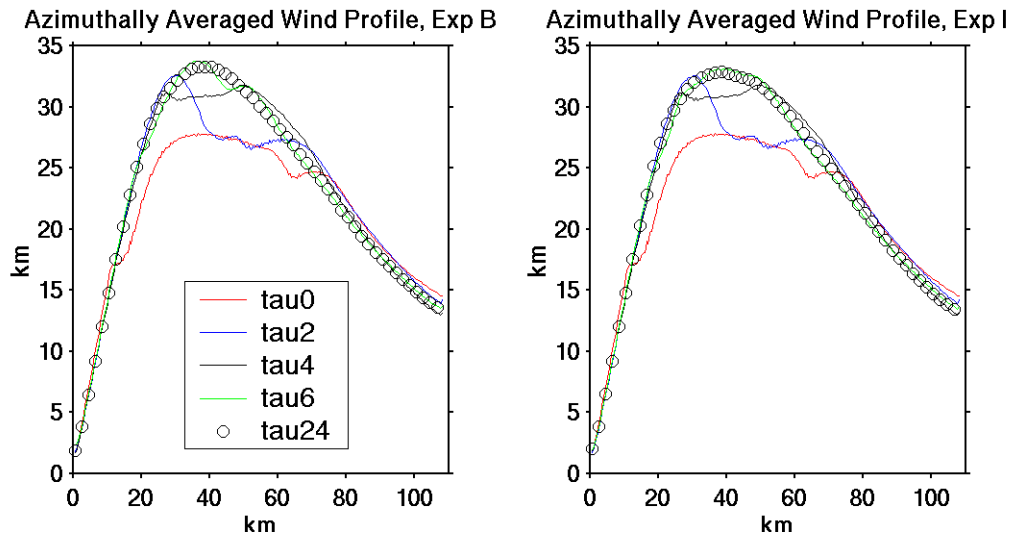
Figure 36. Azimuthally averaged wind profiles for Experiment B (f-plane) and Experiment I (beta plane).

plane case side by side. Just as in the other two beta plane cases, there was no significant difference between the beta plane and *f*-plane experiments. Figure 36 shows that the azimuthally averaged wind profiles are identical as well.

2.   **Larger Vortex on Beta Plane**

Since the effect of beta on a tropical cyclone is sensitive to the flow at a large radius from the center of the vortex (Fiorino and Elsberry, 1989), Experiment J was run with the same initially symmetric monopole as Experiments D and G but with all dimensions doubled to determine whether beta would play a significant role in this larger vortex. This vortex drifted slightly faster than in Experiment G and moved slightly north of west instead of due west, but again there was no significant effect on the vorticity structure. These effects are illustrated in Figure 37. It should be noted that even this double-sized vortex was still small by comparison to most observed in nature. The

Figure 37. Vorticity fields for Experiment J at a) 0 h, b) 24 h, c) 48 h, and d) 72 h. The *f*-plane case is plotted in solid blue lines and the beta plane case in dashed red lines.

Fiorino and Elsberry study showed that the flow outside 300 km from the center of the vortex is most important in determining the effects of beta on tropical cyclone motion. Since the wind in this cyclone dropped to zero inside that radius, the BEP was minimal. Further, this experiment also shows that at this scale, beta has little effect on the tropical cyclone structure.

3.   Model Run with Larger Domain

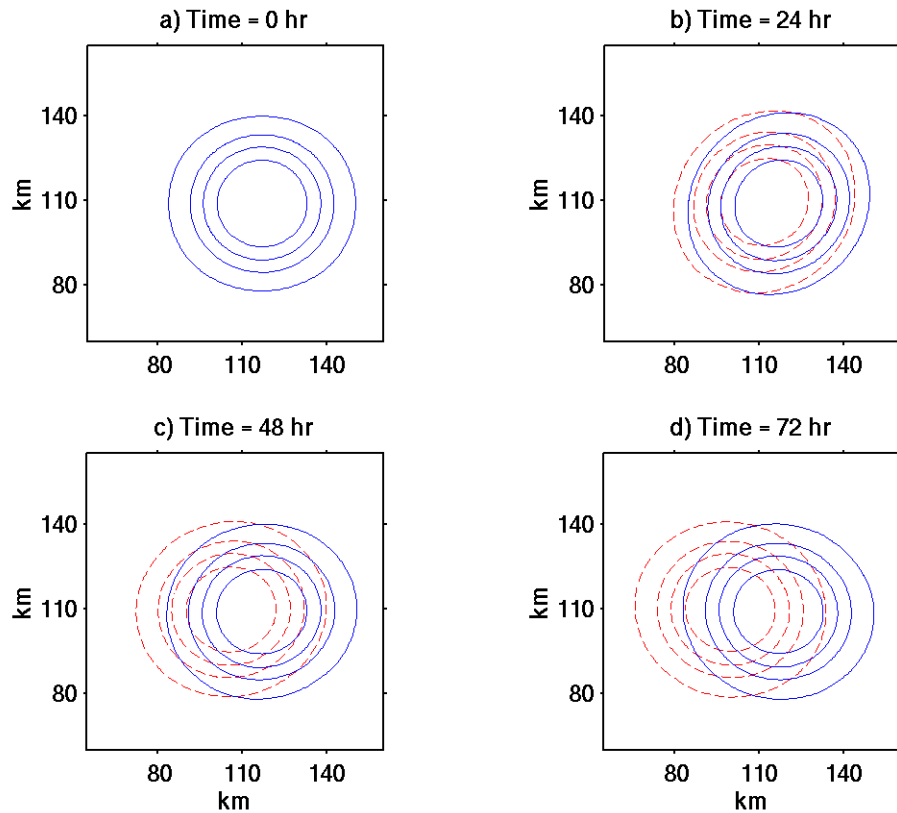Even though the wind speed profile drops off rapidly, the outer portion of the profile does not reach zero (or near zero) inside the 216×216 km domain for the eye experiments. Wind speed does reach zero for the monopole cases, but in the eye cases, which have a higher maximum wind, the wind speed at the outer edge of the domain can be higher than 15 m/s. Though the area examined in this study was the inner 108 km of the vortices, it was considered that interaction with the boundaries might alter the profile inside that area. In order to determine whether this would happen, Experiment B was run on a 648×648 km domain and the wind profile were compared with those of the 216×216 km domain. Since the outer field of slightly negative vorticity was much larger in this case, the central vorticity was decreased from $300 \times 10^5 s^{-1}$ to $230 \times 10^5 s^{-1}$ in order to achieve the same maximum wind speed. Due to these unavoidable differences in initial condition, there were slight differences in the resulting vorticity fields and wind profiles. However, the general shape and evolution of these fields were qualitatively quite similar, indicating that the intersection of the outer field of the vortex with the boundaries did not cause significant errors in the region studied.

4.   Model Runs without Friction

In order to demonstrate the need for viscosity in these experiments, Experiment L was run integrating the same offset monopole as Experiment D without friction. For a case that could run without friction to use as a comparison, Experiment M was run with the initial conditions used by Kuo, et. al. to simulate Typhoon Herb. The initial vorticity field was given by

$$\zeta(r) = \zeta_0 P(r)$$

where the function P is given by

$$P(r) = \begin{cases} 1 - \exp\left[-\dfrac{\kappa}{r}\exp\left(\dfrac{1}{r-1}\right)\right], & \text{if } r < 1; \\ 0, & \text{otherwise} \end{cases}$$

with

$$r = \sqrt{\left(\frac{x-x_0}{a}\right)^2 + \left(\frac{y-y_0}{b}\right)^2}$$

In this case, x_0 and y_0 are the center of the eye, $a = 30$ km, $b = 20$ km, $\kappa = 30$ and $\zeta_0 = 0.003s^{-1}$. Note that this initial vorticity field is very similar to that used in the monopole experiments. Yet, as demonstrated by Figure 38, which shows the vorticity field for Experiments L and M side by side, there is no need for friction as there is in the monopole case. Even without friction, the vorticity field is very smooth at all times while the vorticity evolution of the monopole case without friction is quite ragged. The major difference in these cases is the peakedness term κ which is 30 in the Typhoon Herb case and 2.5609 in the monopole cases. This results in a much more peaked vorticity profile in the monopole cases which leads to greater enstrophy cascade to smaller scales. This cascade continues to smaller and smaller scales until it can no longer be resolved by the model and results in the jagged contours of vorticity. Though this cascade occurs in nature, it must be damped at some scale by turbulence and friction and the viscosity term in the model is an approximation of this damping. Viscosity is also required in the eye cases as the vorticity gradient is even sharper, essential discontinuous, than in the monopole cases.

5. Small Time Scale Examination of Mesovortex Formation

In the offset eye experiments, the vorticity gradient is steeper on one side of the vortex than on the other side. It was considered that one side might therefore be more unstable than the other side. The model was run for one hour with output every five minutes with the same initial conditions as Experiment B. It was thought that the mesovortices may form on the side that is most unstable and then be advected by the mean flow into the less unstable region, thereby acting to redistribute vorticity and facilitate axisymmetrization.

As shown in Figure 39 at 20 minutes, however, the mesovortices do not begin only in the most unstable area, but rather there and exactly opposite that area (180˚ around the vortex). By 40 minutes, also depicted by Figure 39, the mesovortices have spread to lie all the way around the inner wall of the vortex.
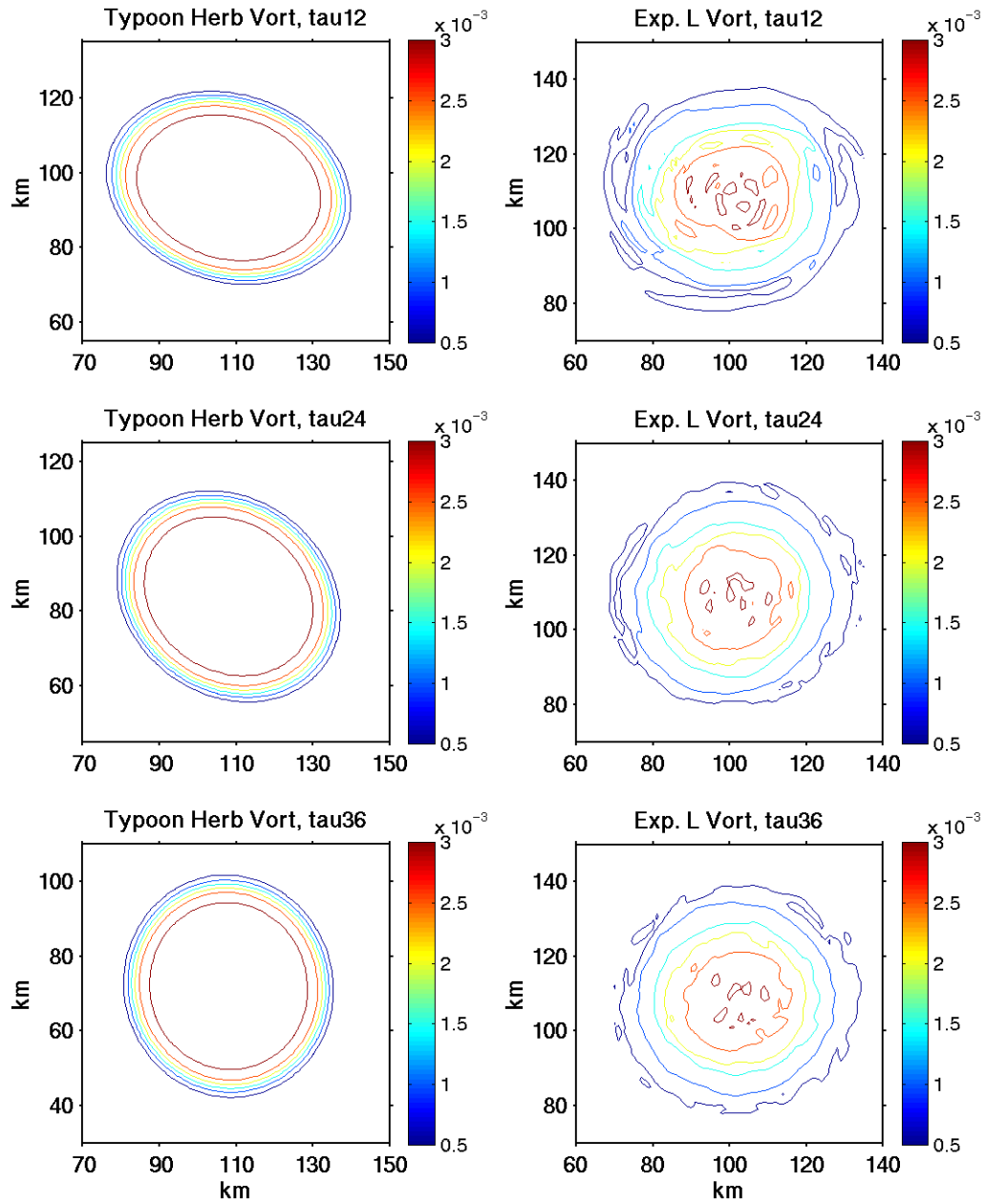

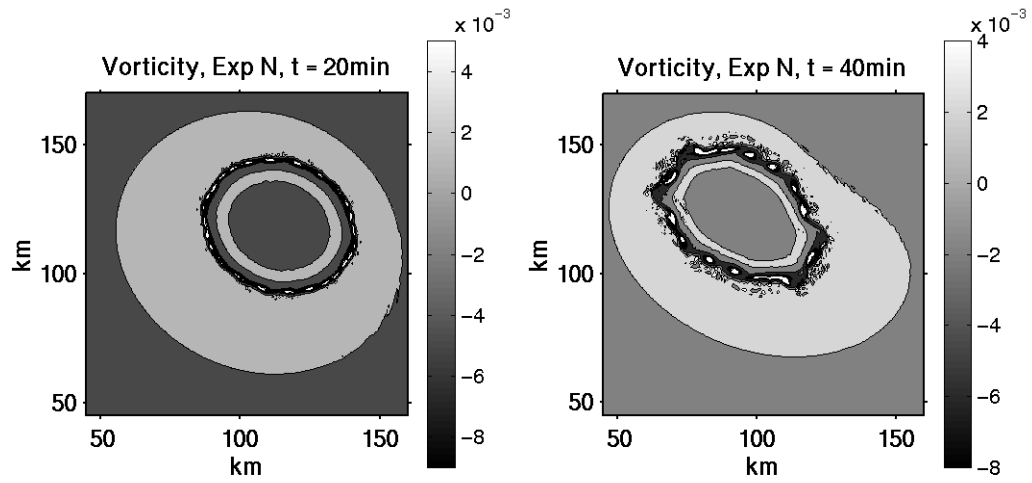Figure 38. Vorticity fields at 12, 24, and 36 h for Typhoon Herb and Experiment L.

Figure 39. Vorticity fields for Experiment N at 20 minutes and 40 minutes.

IV.   CONCLUDING REMARKS

One of the greatest difficulties in conducting a study of this nature is a lack of observations to use in constructing an accurate representation of the potential vorticity field (PKS). Even when long radar records, such as those used by Kuo, et. al. (1999) and Muramatsu (1986), are available, the potential vorticity cannot be calculated since Doppler radar measures tangential wind only, not the radial wind component. As scatterometers cannot accurately measure winds when the seas are confused or in areas where rain is falling (Portabella and Stoffelen, 2001), they are unable to provide wind observations near the center of tropical cyclones. After United States military typhoon reconnaissance flights in the Pacific were discontinued in 1987 (Weatherford and Gray, 1988), even fewer observations are available. Since the mesovortices found in this and other studies form and dissipate so quickly, verification and careful study of them would require observations of a higher temporal resolution than even the aircraft observations that are made in the Atlantic. New techniques for inferring wind near the tropopause in the inner core region and near the surface inside the eye from GOES one-minute interval imagery now show promise at filling some of this observational void (Hasler, 1998). Unfortunately, these techniques cannot be taken advantage of until more routine sequences of one-minute interval imagery are taken.

In this study, a non-divergent barotropic spectral model was used to examine the axisymmetrization process in tropical cyclones, the accompanying transfers of kinetic energy between scales, and to assess their impact on changing the intensity and strength of the cyclone. Admittedly, the processes that intensify a tropical cyclone are more complex than those that can be represented by the model. However, studying the conservation processes in the absence of complete physics allows us to determine which process is responsible for the resulting effects. Any change in kinetic energy must be due to transfer of energy from one scale to another, as the model does not represent internal energy, potential energy, or any conversion from those types of energy to kinetic energy.

The evolution of the vorticity structure proceeded much as described in previous works by PKS and Schubert, et. al. (1999). In the offset eye cases, symmetrization

occurred primarily through strong mixing due to barotropic instability. The monopole cases developed spiral bands which subsequently broke off on the ends, mixing vorticity outward.

Beta plane cases were run and differences between the *f*-plane and beta plane results compared. The inclusion of beta was found to cause only insignificant differences in the vorticity evolution. There was, however, a greater difference between the *f*-plane and beta plane cases for the more unstable offset eye cases than on the monopole cases. There was no difference in the resulting winds from *f*-plane and beta plane integrations.

Since no addition of latent heat is provided in the model, as occurs in nature, no significant intensification of the tropical cyclones was expected. In fact, if maximum wind is used to quantify intensity, each of these cases weakened. However, transfers of kinetic energy from the mean flow to the asymmetries were observed as mesovortices formed and transfers from the asymmetries back to the mean flow as axisymmetrization proceeded. The formation of these mesovortices and the accompanying transfer of kinetic energy occurred very quickly, typically in less than one hour. Their disappearance and transfer of energy back to the mean flow occurred in a few hours. The transfer of kinetic energy from the asymmetry to the mean flow caused an increase in the azimuthally averaged wind over a band over 70 km wide in the eye cases. Even though the maximum wind in the cyclone did not increase, the maximum azimuthally averaged wind did increase, indicating that symmetrization does play a role in increasing the strength of a tropical cyclone. Symmetrization of the offset monopole cases also resulted in increased azimuthally averaged wind, though both the magnitude of the increase and the width of the band over which it occurred were less than in the off-center eye cases. While moist processes and boundary layer dynamics are certainly important in the intensification of a tropical cyclone, this work has shown that symmetrization of an asymmetric structure also plays a role in building tropical cyclone strength.

LIST OF REFERENCES

Bosart, L. F., C. S. Velden, W. E. Bracken, J. Molinari, and P. G. Black, 2000: Environmental influences on the rapid intensification of Hurricane Opal (1995) over the Gulf of Mexico. *Mon. Wea. Rev.,* **128**, 322-350.

Chan, J. C. L, and R. T. Williams, 1987: Analytical and numerical studies of the beta-effect in tropical cyclone motion. Part I: Zero mean flow. *J. Atmos. Sci.*, **44**, 1257-1265.

Chen, Y., and M. K. Yau, 2001: Spiral bands in a simulated hurricane. Part I: Vortex Rossby wave verification. *J. Atmos. Sci.*, **58**, 2128-2145.

Fiorino, M., R. L. Elsberry, 1989: Some aspects of vortex structure related to tropical cyclone motion. *J. Atmos. Sci.*, **46**, 975–990.

Foley, G. R., 1995: Observations and analysis of tropical cyclones. *Global Perspectives on Tropical Cyclones*. WMO/TD-No. 693. Report No. TCP-38, 1-18.

Fulton, S. R., and W. H. Schubert, 1987: Chebyshev spectral methods for limited-area models. Part I: Model problem analysis. *Mon. Wea. Rev.,* **115**, 1940-1953.

Hasler, A. F., K. Palaniappan, C. Kambhammetu, P. Black, E. Uhlhorn, and D. Chesters, 1998: High-resolution wind fields within the inner core and eye of a mature tropical cyclone from GOES 1-min images. *Bull. Amer. Meteor. Soc.*, **79**, 2483-2496.

Kossin, J. P., and W. H. Schubert, 2001: Mesovortices, polygonal flow patterns, and rapid pressure falls in hurricane-like vortices. *J. Atmos. Sci.*, **58**, 2196-2209.

Kuo, H. C., J. H. Chen, R. T. Williams, and C. P. Chang, 2001: Rossby waves in zonally opposing mean flow: Behavior in northwest Pacific summer monsoon. *J. Atmos. Sci.*, **58**, 1035-1050.

Kuo, H. C., R. T. Williams, and J. H. Chen, 1999,: A possible mechanism for the eye rotation of Typhoon Herb. *J. Atmos. Sci.*, **56**, 1659-1673.

Kuo, H. C., and W. H. Schubert, 1988: Stability of cloud-topped boundary layers. *Quart. J. Roy. Meteor. Soc.*, **114**, 887-916.

Kurihara, Y., 1976: On the development of spiral bands in a tropical cyclone. *J. Atmos. Sci.*, **33**, 940-958.

Lamb, H., 1932: Hydrodynamics. 6th ed. Dover, 732 pp.

Lewis, B. M., and H. F. Hawkins, 1982: Polygonal eye walls and rainbands in hurricanes. *Bull. Amer. Meteor. Soc*., **63**, 1294-1300.

Lorenz, E. N., 1960: Energy and numerical weather prediction. *Tellus XII*, **4**, 364-373.

Muramatsu, T., 1986: The structure of polygonal eye of a typhoon. *J. Meteor. Soc. Japan*, **64**, 913-921.

Orszag, S. A., 1971a: Galerkin approximations to flows within slabs, spheres, and cylinders, *Phys. Rev. Lett.,* **26**, 1100-1103.

Orszag, S. A., 1971b: Numerical simulation of incompressible flows within simple boundaries. I. Galerkin (spectral) representations. *Stud. Appl. Math*., **50**, 293-327.

Orszag, S. A., and M. Israeli, 1974: Numerical simulation of viscous incompressible flows. *Ann. Rev. Fluid Mech*., **6**, 281-318.

Portabella, M., and A. Stoffelen, 2001: Rain detection and quality control of sea winds. *J. Atmos. Oceanic Technol*., **18**, 1171-1183.

Prieto, R., J. P. Kossin, and W. H. Schubert, 2001: Symmetrization of lopsided vorticity monopoles and offset hurricane eyes. *Quart. J. Roy. Meteor. Soc.*, **127**, 1-17.

Schubert, W. H., M. T. Montgomery, R. K. Taft, T. A. Guinn, S. R. Fulton, J. P. Kossin, and J. P. Edwards, 1999: Polygonal Eyewalls, asymmetric eye contraction, and potential vorticity mixing in hurricanes. *J. Atmos. Sci*., **56**, 1197-1223.

Thomson, W., 1880: Vibrations of a columnar vortex. *Phil. Mag.*, **10**, 155-168.

Weatherford, C. L., and W. M. Gray, 1988: Typhoon structure as revealed by aircraft reconnaissance. Part I: Data analysis and climatology. *Mon. Wea. Rev*., **116**, 1032-1043.

Willoughby, H. E., 1978: A possible mechanism for the formation of hurricane rainbands. *J. Atmos. Sci*., **35**, 836-848.

INITIAL DISTRIBUTION LIST

1.   Defense Technical Information Center
   8725 John J. Kingman Road, Suite 0944
   Ft. Belvoir, Virginia 22060-6218

2.   Dudley Knox Library
   Naval Postgraduate School
   411 Dyer Road
   Monterey, California 93943-5101

3.   Dr. Roger T. Williams
   Code MR/Wu
   Naval Postgraduate School
   589 Dyer Road, Rm 254
   Monterey, California 93943-5114

4.   Dr. Chih-Pei Chang
   Code MR/Cp
   Naval Postgraduate School
   589 Dyer Road, Rm 254
   Monterey, California 93943-5114

5.   Dr. Hung-Chi Kuo
   Department of Atmospheric Sciences
   National Taiwan University
   No. 61, Lane 144, Sec. 4, Keelung Road
   Taipei, Taiwan, R.O.C.

6.   Dr. Russell L. Elsberry
   Code MR/Es
   Naval Postgraduate School
   589 Dyer Road, Rm 254
   Monterey, California 93943-5114

7.   Dr. Patrick A. Harr
   Code MR/Hp
   Naval Postgraduate School
   589 Dyer Road, Rm 254
   Monterey, California 93943-5114

8.   Dr. Wayne H. Schubert
   Department of Atmospheric Science
   Colorado State University
   Fort Collins, Colorado 80523